Drosophila sperm development and intercellular cytoplasm sharing through ring canals do not require an intact fusome

Ronit S. Kaufman (1)*, Kari L. Price (1)*, Katelynn M. Mannix (1), Kathleen M. Ayers (1), Andrew M. Hudson (1), Lynn Cooley (1,2,3)

1. Department of Genetics, Yale University School of Medicine, New Haven, CT
2. Department of Cell Biology, Yale University School of Medicine, New Haven CT
3. Department of Molecular, Cellular & Developmental Biology, Yale University, New Haven, CT
*Equal contribution

Lead contact (lynn.cooley@yale.edu)

Abstract

Animal germ cells communicate directly with each other during gametogenesis through intercellular bridges, often called ring canals (RCs), that form as a consequence of incomplete cytokinesis during cell division. Developing germ cells in Drosophila have an additional specialized organelle connecting the cells called the fusome. Ring canals and the fusome are required for fertility in Drosophila females, but little is known about their roles during spermatogenesis. With live imaging, we directly observe the intercellular movement of GFP and a subset of endogenous proteins through RCs during spermatogenesis, from two-cell diploid spermatogonia to clusters of 64 post-meiotic haploid spermatids, demonstrating that RCs are stable and open to intercellular traffic throughout spermatogenesis. Disruption of the fusome, a large cytoplasmic structure that extends through RCs and is important during oogenesis, had no effect on spermatogenesis or male fertility under normal conditions. Our results reveal that male germline RCs allow the sharing of cytoplasmic information that might play a role in quality control surveillance during sperm development.

Keywords

Drosophila spermatogenesis, ring canal, fusome, intercellular movement

Introduction

Germ cells throughout the animal kingdom maintain direct cytoplasmic intercellular connections during gametogenesis. Germ cell intercellular bridges (ICBs) were first observed in cat testes by electron microscopy that revealed channels connecting spermatids of ~1 micron in diameter lined with an electron dense plasma membrane compartment (Burgos & Fawcett, 1955). Subsequent reports described similar ICBs in other species, ranging from Hydra to mammals (Dym & Fawcett, 1971; Fawcett et al., 1959).

In Drosophila, intercellular bridges are called ring canals (RCs) and were first discovered in ovarian germline cells (Brown & Smith, 1964; Koch & King, 1966; Koch & King, 1969) where they are essential for oocyte growth during oogenesis (Greenbaum et al., 2011; Robinson & Cooley, 1996). Moreover, previous work from our lab has shown that RCs in Drosophila somatic ovarian follicle cells allow movement of cytoplasmic contents between connected cells (Airoldi et al., 2011) that contributes to protein level equilibration (McLean & Cooley, 2013). In contrast, the functional significance of male RCs during spermatogenesis remains less well characterized.

During Drosophila spermatogenesis, germline stem cells (GSCs) located at the hub of the testis divide asymmetrically to produce another GSC and a spermatogonial cell that divides mitotically four times to form a cluster of 16 primary spermatocytes connected by RCs (Figure 1A', B'). Mature spermatocytes enter meiosis synchronously to produce 64 spermatids that remain connected by RCs (Figure 1A") (Fuller, 1993; Hime et al., 1996). RCs form as the result of incomplete cytokinesis during mitotic and meiotic cell divisions during which cleavage furrows ingress but do not complete the final cytokinetic step of abscission leaving bridges of 1-2 microns in diameter (Figure 1B-B'). Spermatids remain connected via RCs during the subsequent processes of spermatid tail elongation and individualization that are required for the production of mature, motile spermatozoa (Figure 1B-B'). Proteins identified at RCs include several that persist from cleavage furrows during cytokinesis as well as proteins recruited after furrow ingression. Unlike the actin-rich intercellular bridges in male mice or Drosophila females, Drosophila male germline RCs have a septin-rich cytoskeleton, which includes Pnut, Sep1, and Sep2, in addition to Pavarotti (Pav, a kinesin-like protein) and its obligate binding partner Tumbleweed (a RacGAP), the cytoskeletal scaffolding proteins Cindr and Anillin, Nessun dorma, and Orbit/CLASP (for review, see Haglund et al., 2011; Lu et al., 2017; Yamashita, 2018).

In addition to RCs, cells within a cyst are connected by the fusome: a large, branched organelle that extends through each RC in the cyst (Figure 1B and 1B"). Fusomes contain several cytoskeletal proteins, including α- and β-Spectrin, as well as Adducin (encoded by the *hu-li tai shao* (*hts*) gene) (De Cuevas et al., 1996; Lin et al., 1994; Yue & Spradling, 1992), all three of which are otherwise cortically located in somatic cells. In electron micrographs of Drosophila ovaries, fusomes exclude most ribosomes and mitochondria and also contain abundant endoplasmic reticulum (ER) cisternae (Lin et al., 1994). Several ER proteins are concentrated in female fusomes including PDI, Sec61α, Rtnl1 and TER94 as well as the KDEL ER reporter (León & McKearin, 1999; Lighthouse et al., 2008; Röper, 2007; Snapp et al., 2004). In females, the fusome disappears soon after cells exit the mitotic cell cycle during oogenesis. Genetic analysis has shown that the fusome is necessary to orient mitotic spindles during cell division and to mediate the transfer of mRNAs and proteins into the pro-oocyte from nurse cells during oocyte specification (De Cuevas et al., 1996; Lin et al., 1994; Lin & Spradling, 1995; McKearin & Ohlstein, 1995). Mutations in the *hts* gene cause egg chamber arrest and female sterility.

The fusomes in males differ from female fusomes both in their composition and how long they persist during gametogenesis. The same ER proteins found in female fusomes are not concentrated in the male fusome (Lighthouse et al., 2008). The male fusome does not disappear after the completion of spermatogonial mitotic divisions; instead, it grows with each meiotic division and persists throughout spermatogenesis, including during spermatid elongation (Figure 1B", bottom inset), where it has been proposed to gather RCs to the distal tip of elongating spermatids (Hime et al., 1996). The male fusome has been implicated in the coordinated cell death response of germ cell cysts to DNA damage (Lu & Yamashita, 2017). However, the extent to which the fusome is required for sperm development under normal conditions remains unclear.

Here, using a combination of extensive live cell imaging, genetics, and electron microscopy, we explored the function of Drosophila male germline RCs and fusomes during spermatogenesis. We directly observed movement of GFP and endogenous proteins through RCs. Movement between neighboring cells within a germline cyst occurred throughout all stages of spermatogenesis, including post-meiotically, and independently of protein size. Further, we found that fusome disruption specifically in male germline cells did not have a major effect on fertility, RC formation, or intercellular protein movement.

Results

RCs allow intercellular movement of proteins in mitotic spermatogonial cells

To investigate intercellular protein movement in the Drosophila testis, we expressed photoactivatable GFP (PA-GFP) (Pfeiffer et al., 2012) using *nos-* or *bam-Gal4* drivers in germline cells also expressing GFP-tagged Pav (Pav::GFP) to mark RCs. Following activation in a single cell within a spermatogonial cyst, we captured time-lapse movies of PA-GFP localization (Figure 2, Supplemental Movie 1-4). Within 30 seconds following photoactivation, we observed movement of PA-GFP from the activated cell through RCs to other cells within mitotically active cysts (Figure 2A-L). Within 10 minutes following photoactivation, we observed GFP signal throughout most, if not all, cells in all spermatogonial cysts from 2-cell through 16-cell cysts (Figure 2M-P, n=94). These data demonstrate that RCs are persistent open channels that allow diffusion of GFP between spermatogonial cells.

To examine the movement of endogenous Drosophila proteins through RCs, we performed Fluorescence Loss in Photobleaching (FLIP) experiments in 16-cell post-mitotic spermatocyte cysts expressing either GFP or GFP-fusion proteins. We selected FlyTrap lines with GFP-tagged proteins (Buszczak et al., 2007; Lowe et al., 2014; Nagarkar-Jaiswal et al., 2015; Quiñones-Coello et al., 2007) that had high GFP-expression in the male germline (Figure S1, S2) or had been previously assayed for movement in female somatic follicle cells (Airoldi et al., 2011). A region of interest was repeatedly photobleached while we simultaneously captured images of the GFP fluorescence in the entire cyst. Movement of proteins into the bleaching zone was determined by a loss of GFP fluorescence in neighboring cells. We first demonstrated by FLIP that, consistent with PA-GFP results, cytoplasmically expressed GFP moved through the RCs (Figure 3A-C, M). Similarly, we observed movement of several GFP-fusion proteins including Kra, Oda, Men-B, and β-Tub56D (Figure 3D-I, Table 1). However, we did not detect movement of most of the selected GFP-fusion proteins within the 60 minute time-frame (n=2-4 cysts per genotype; Table 1). The sizes of the different proteins did not appear to correlate with the ability to move through the RCs between the cells. Remarkably, GFP::CaM, which we previously showed moves through RCs in female follicle cells (Airoldi et al., 2011), did not move between male germline cells (Figure 3J-L, P). These, albeit limited, data indicate that only a subset of proteins freely diffuses between cells despite the open RCs and suggest that there are some, as of yet unknown, criteria for this ability to move.

Proteins can move between cells in meiotic and post-meiotic cysts

One hypothesis for the function of RCs during spermatogenesis is to allow sharing of X-linked gene products to Y-bearing cells after meiosis (Braun et al., 1989; Morales et al., 2002). To assess post-meiotic sharing, we performed photoactivation studies in meiotic and post-meiotic cysts as well as haploid spermatids in the same manner as before. One notable difference, however, is that in the later stages multiple cells, rather than a single cell, were irradiated to increase the amount of visible PA-GFP in the smaller cells. In 32- and 64-cell cysts, where we illuminated cells in two separate locations, we could easily detect the spread of photoactivated PA-GFP between cells within 10 minutes following photoactivation (Figure 4A-F, Supplemental Movie 5-6). Interestingly, not all of the cells of the post-meiotic cysts were fluorescent after 10 minutes of imaging (Figure 4C, F). This is most likely because the ratio of photoactivated GFP to overall cyst size is smaller in the post-meiotic cells than in the earlier cysts and diffused GFP becomes undetectable further away from the original region of activation. Additionally, we performed FLIP on endogenous GFP-tagged proteins in 64-cell cysts, and found their ability to move between cells just as we observed in primary spermatocytes (GFP::Men-B shown in Figure 4J-L).

Finally, we tracked movement of PA-GFP in elongated spermatids after activation in a central zone of a spermatid bundle. We observed the spreading of GFP along the length of the bundle and to outer spermatids (Figure 4G-I, Supplemental Movie 7). Since RCs were located at one end of the spermatid bundle (Figure 4I, arrow), GFP would need to reach RCs before spreading to lateral cells. However, in addition to the RCs, elongated spermatids contain lateral membrane perforations throughout the length of the tails (Fabrizio et al., 1998; Tokuyasu et al., 1972), making it possible that GFP moved laterally through the perforations independent of RCs (Figure 4M). To investigate protein movement further, we carefully tracked the spread of PA-GFP over a period of 10 minutes following activation (Figure 4N-S). We reasoned that if movement to lateral cells depends on RCs, GFP fluorescence would increase near RCs (Figure 4O, region 4) before it accumulated at a location directly lateral to the activation zone (Figure 4O, region 5). In all samples examined (n=3), PA-GFP was first observed nearest the RCs, in region 4 (Figure 4P, U; Figure S3). Although we cannot rule out some lateral movement through perforations, these data suggest that intercellular movement is predominantly through RCs (Figure 4T). Our observation of intercellular protein movement during and after meiosis and during spermatid tail elongation provides evidence that developing sperm are in direct communication throughout spermatogenesis.

RNAi inhibition of *αSpectrin* or Adducin severely disrupts fusome structure

During Drosophila oogenesis, the fusome is necessary for the production of viable gametes but its role in spermatogenesis remains largely unknown (De Cuevas & Spradling, 1998; Lin et al., 1994). To investigate the role of the fusome in males, we carried out germline-specific RNAi of genes encoding two structural proteins in the fusome: *αSpectrin* and Adducin (encoded by the *hts* gene). Using a Pav::GFP background to mark RCs, we used two different Gal4 drivers to express these RNAi lines throughout development and in adults: *nos-Gal4*, which expresses in the early mitotic stages, or *bam-Gal4*, which begins expression in 8-cell cysts (Lu & Yamashita, 2017). We stained control, *αSpectrin* knockdown, and *hts* knockdown testes with antibodies to either αSpectrin (3A9) or Adducin (Hts1B1) to monitor the fusome by immunofluorescence.

In wild-type testes, the fusome was present throughout all stages of spermatogenesis and extended through RCs connecting all cells within a cyst, and was present at the growing end of spermatid tails (Figure 5A-E). In both *nos>* and *bam>αSpec RNAi* testes, we did not detect either Adducin (Figure 5F-J, S4) or αSpectrin (Figure S5-6) fusome labeling in the mitotic region where *nos* and *bam* are expressed (Figure 5F,G, Zone 1), indicating the fusome was disrupted. We did, however, observe Adducin cortically at membranes in *nos>* and *bam>αSpec RNAi* testes and in elongating spermatid tails (Figure 5G, I, S4H). In both genotypes, αSpectrin protein remained absent from a fusome structure in Zones 2 and 3 (Figure S5-6), demonstrating the long-term effectiveness of RNAi driven by *nos-Gal4* and *bam-Gal4*. Interestingly, in both *nos>* and *bam>αSpec RNAi* testes, we did observe Adducin-containing fusome-like fragments in primary spermatocytes (Figure 5H, Zone 2) and in meiotically dividing spermatocytes (Figure 5J, Zone 3), despite the absence of *α*Spectrin. Only a small subset of the fusome-like fragments was associated with RCs (Figure 5H", inset). These results suggested that cells began accumulating Adducin in fusome-like fragments independent of *α*Spectrin in post-mitotic cysts.

We also examined *nos>* and *bam>hts RNAi* testes stained with either Adducin or αSpectrin. In *nos>hts RNAi* testes, the fusome was effectively disrupted in the mitotic region but Adducin- and αSpectrin-containing fusome fragments were present outside of the zone of *nos* expression, in Zones 2 and 3 (data not shown). In *bam>hts RNAi* testes, fusome morphology in Zone 1 was indistinguishable from control testes. In Zones 2 and 3, Adducin-containing fusome fragments were observed in addition to Adducin at the growing ends of spermatid tails (Figure S7D). Similarly, we observed αSpectrin-labeled fusome-like fragments in Zones 2 and 3 in *bam>hts RNAi* and at the growing ends of spermatid tails (data not shown). Surprisingly, despite the absence of an intact fusome, overall testis morphology appeared normal (Figure 5F).

As *nos>αSpec RNAi* gave a more complete knockdown of the fusome, we used this genotype to assess the effect of fusome disruption. We examined Pav::GFP in *nos>αSpec RNAi* testes to determine whether fusome disruption had an effect on RC formation. We found that fusome disruption did not affect accumulation of Pav::GFP to RCs (compare Figures 5C' and 5H'), and that the diameters of the RCs in wild-type and fusome-compromised testes were not statistically different (p=0.98); RCs were the same diameter, ~ 1.6 μm, in both wild-type (n=300) and *nos>αSpec RNAi* (n=201) throughout spermatogenesis. However, 11.1% of RCs in the

nos>aSpec RNAi spermatogonia and primary spermatocytes appeared morphologically abnormal (not round; Figure 5H inset) or collapsed (having no obvious lumen; Figure S8) suggesting that the fusome may play a role in RC stability.

To assess the extent of fusome disruption at greater resolution, we performed electron microscopy on *hts*[ΔG] or *aSpec RNAi* testes driven by *nos-Gal4*. RCs were easily identifiable in cross-section by their electron dense plasma membranes (Figure 6A-D, Figure S9A-C). In wild-type testes, the fusome appeared as a region of ribosome- and mitochondria-free cytoplasm that extended through the RCs (n=12) (Figure 6A, A', purple shading in A') and between connecting cells. We also observed ER-like vesicles frequently embedded in the fusome, similar to electron micrographs of Drosophila ovaries (Lin et al., 1994). In *nos>aSpec* (n=12; Figure 6C, D) and *hts*[ΔG] (n=5; Figure S9C) samples, we did not observe the characteristic ribosome-free cytoplasmic compartment within RC lumens.

To quantify the loss of the fusome in RNAi cells, we measured the ribosome density in cytoplasm within the RC lumen compared to cytoplasm outside of the RC lumen. To do this, we obtained the standard deviation (SD) of the mean pixel intensity from three non-overlapping 40 μm² regions-of-interest (ROI) in the RC lumen (Figure 6B, D; "RC"; blue) or cytoplasm distant from the RC lumen (Figure 6B, D; "non-RC"; orange) in electron micrographs (see Figure S10 for ROIs). We averaged the three values corresponding to each cellular compartment. In the cytoplasm of control RCs, the average SD was 22.30±3.5, and in the non-RC cytoplasm the average SD was 27.53±4.2 (p=0.0083, two-tailed student's t-test) (Figure 6E). The higher SD in the non-RC cytoplasm represents a broader distribution of pixel intensity values, which corresponds to the presence of electron-dense ribosomes. In contrast, the lower SD in the RC lumen cytoplasm corresponds to the observed reduction in electron-dense ribosomes that marks the fusome. We performed these same analyses in *nos>aSpec RNAi* RCs and observed that the SDs of RC and non-RC cytoplasm were not statistically different with average SD values of 26.32±4.1 and 26.24±4.2, respectively (Figure 6E, p=0.96).

Fusome disruption has minimal impact on male fertility

We evaluated the effect of fusome disruption on male fertility by comparing wild-type fertility rates to males with *aSpec* or *hts RNAi*. We detected little discernible effect on male fertility in males lacking an intact fusome (Figure S11A). This was unexpected since previous work had reported male sterility caused by the *hts*[1103] mutation (Wilson, 2005). Upon testing, we found that male fertility of three *hts* alleles was dramatically reduced (Figure S11B). Two *hts* alleles, *hts*[1103] and *hts*[1], displayed declining progeny counts over a 14-day period, whereas *hts*[ΔG] and *hts*[W532X] produced very few progeny throughout the same time-frame (Figure S11C). Given the marked reduction in fertility rate in *hts* mutants, but negligible effect of germline-specific inhibition of *hts* expression, we posit that the sterility of *hts* mutant males may be caused by a fusome-independent function of Adducin. As previously mentioned, in both aSpectrin and Hts knockdown testes, Adducin localization to fusome fragments in the post mitotic and meiotic zones (Zones 2 and 3) as well as elongating spermatid tails may suggest that any remaining Adducin protein is sufficient for normal fertility, despite overt fusome disruption.

The results of our examination of germline-specific RNAi directed to structural components of the fusome when taken together, demonstrate that intact fusomes are not necessary for spermatogenesis in normal, unchallenged, conditions. This is in stark contrast to Drosophila oogenesis where disruption of fusomes results in oogenesis arrest and sterility (Huynh & St Johnston, 2004).

The fusome is not necessary for movement of GFP between cells

Studies in Drosophila oogenesis demonstrated a requirement for the fusome in the sharing of cytoplasmic information among the germ cells within a cyst (Yue & Spradling, 1992). However, as the fusome was not required for male fertility, we explored whether disruption of the fusome had an impact on protein movement through the RCs during spermatogenesis. We activated PA-GFP in *aSpec RNAi* testes and monitored the movement of cytoplasmic GFP (Figure 7, Supplemental Movie 8-9). After photoactivation in a single cell, PA-GFP moved to neighboring cells in 2-, 4-, and 16-cell cysts, just as in wild-type testes, and on a similar time scale (n=93) (Figure 7A-F). Similarly, movement of PA-GFP through the RCs in post-meiotic cells was not

impacted by disruption of the fusome (Figure 7G-I, Supplemental Movie 10). Moreover, FLIP analysis in a fusome knockdown background showed that, as in wild-type testes, GFP::Oda did move between cells whereas GFP::CaM did not (data not shown). To determine if the rate of GFP diffusion between cells was affected by fusome disruption, we analyzed the diffusion of GFP from one cell into another. From 16-cell cysts, we isolated groups of two cells connected by a single RC in which we could measure the diffusion of total GFP from one cell directly into another cell in the presence of the fusome versus in fusome knockdown cells (Figure S12).The initial rate of diffusion was slightly faster in fusome knockdown cells (Figure S12), suggesting the possibility that the fusome moderates the rate of cytoplasm exchange between cells. In sum, our data suggest the fusome is not necessary to mediate transport between the cells in a cyst during spermatogenesis though it may modulate the rate of diffusion between cells.

Discussion

Interconnectivity is a major feature during Drosophila spermatogenesis, involving at least three types of intra-cyst cellular connections: ring canals, the fusome, and lateral perforations in post-meiotic spermatid tails. Our data could support hypotheses that these cells maintain extensive connectivity for quality control under stress (Lu & Yamashita, 2017), synchronizing signals that govern cell cycling, (Fuller, 1993; Gärthner et al., 2014; Huckins & Oakberg, 1978; Ren & Russell, 1991), and sharing of X- or Y-linked genes products in post-meiotic cells (Braun et al., 1989). We have demonstrated that RCs are open channels for protein sharing throughout all the stages of spermatogenesis, and that GFP and some endogenous proteins travel readily between connected cells. Under normal laboratory conditions, our data show the fusome is not required for spermatogenesis since compromising it does not impair RC formation, overall testis morphology, or male fertility. The fusome may function instead in response to abnormal conditions - a synchronous "all-or-none" cell death response of spermatogonial cysts in response to DNA damage involves the fusome (Lu & Yamashita, 2017).

This work represents the first extensive evidence that RCs mediate the sharing of cytoplasmic components throughout the entire process of Drosophila spermatogenesis, highlighting their role in cell-cell communication and protein sharing in differentiating male germline cells. Using live-imaging approaches, we documented diffusion of GFP and endogenous proteins through RCs in all stages, including post-meiotically. In post-meiotic haploid spermatid bundles, ring canals are located at the opposite end of the cell from the nuclei, yet we observed rapid GFP diffusion along the length of bundles, and spreading to neighboring cells, primarily through RCs. We cannot rule out protein sharing via lateral perforations between spermatid tails; however, tracking of GFP indicates the faster route relies on RCs (Figures 4 and S3).

Interestingly, protein size does not appear to correlate with its ability to move into neighboring cells. Within the time frame of our live imaging experiments, proteins ranging from 28 to 69 kDa moved through RCs, while many proteins in the same range of molecular mass did not (Table 1). These results are similar to our assessment of movement across the smaller RCs connecting somatic follicle cells in Drosophila egg chambers (Airoldi et al., 2011). An unexpected difference is that GFP-tagged Calmodulin (CaM), a 17 kDa calcium binding messenger protein, moved freely through ovarian follicle cell RCs, but not through testis RCs. Previous work has shown differences in CaM diffusion rates depending on whether CaM is bound to other complexes or immobile structures (Sanabria et al., 2008). The ability of proteins to diffuse between cells may be dependent on whether they are associated with a larger complex, an organelle, or the cytoskeleton. This could suggest that CaM in the testis, but not in the ovarian follicle cells, is part of a larger complex.

Our work supports the long-held idea that male RCs are required to allow post-meiotic sharing of X- or Y-linked gene products between haploid cells. While active biosynthesis of crucial mRNAs and proteins occurs during the 3-day growth phase of the primary spermatocytes prior to meiosis (Fuller, 1993), a subset of genes, called "cup" and "comet" genes based on the localization of mRNAs clustered at one end of spermatid bundles, is transcribed only after meiosis during spermatid tail elongation (Barreau et al., 2008; Jandura et al., 2017). The timing of cup and comet gene expression suggests they function during spermatid development. Mutants of one comet gene, *scotti*, which is involved in spermatid individualization, are male sterile (Barreau et al., 2008). Since *scotti* heterozygotes are fertile, products made in haploid spermatids with the wild-type allele likely spread to spermatids with the mutant allele (White-Cooper, 2010). Although this equilibration could be mediated by lateral perforations between spermatid tails (Fabrizio et al., 1998; Tokuyasu et al., 1972), our work

suggests the most efficient path between cells is through RCs. This would be especially critical for products of post-meiotically expressed X-linked genes such as *r-cup* and *p-cup*. Our evidence of protein exchange through RCs even during post-meiotic stages of spermatogenesis demonstrates that haploid cells are indeed able to share gene products with their neighbors.

In addition to RCs, Drosophila male germline cells contain fusomes, which provide another type of connectivity between cells. We dramatically disrupted fusomes by RNAi inhibition of structural components and found negligible effects on fertility. Furthermore, the rate of movement of GFP between cells lacking fusomes was unchanged, suggesting that fusomes are not needed to either promote or prevent protein movement through RCs under normal conditions. Discovering that compromising fusomes has little effect on spermatogenesis was unexpected since disruption of fusomes in ovaries causes egg chamber arrest and female sterility (Lin et al., 1994; Yan et al., 2014). The composition of fusomes is also different in males and females; while they share some cytoskeletal proteins (αSpectrin, Adducin, Ankyrin), female fusomes are richer in endoplasmic reticulum (ER) membranes and ER proteins (De Cuevas et al., 1997; Hime et al., 1996; Lighthouse et al., 2008; Lu et al., 2017; Snapp et al., 2004; Yamashita, 2018).

The striking functional difference between male and female fusomes may reflect the role of the fusome in breaking symmetry early in oogenesis. While male fusomes persist throughout spermatogenesis, (Hime et al., 1996) female fusomes are present only in the cystoblast stage of development where they have been implicated in mitotic spindle orientation, cell cycle control, and oocyte specification (De Cuevas & Spradling, 1998; Deng & Lin, 1997; Lilly et al., 2000; Lin et al., 1994; Lin & Spradling, 1995; McGrail & Hays, 1997; Yamashita, 2018). Female fusome disassembly begins immediately after the completion of mitotic divisions in the ovary. As the fusome fades, a polarized microtubule cytoskeleton forms in its place that promotes oocyte fate for one of the sixteen sibling cells with the rest becoming nurse cells (Grieder et al., 2000; McGrail & Hays, 1997; Theurkauf et al., 1993). In contrast, all 16 post-mitotic cells of male cysts proceed to meiosis and produce 64 sperm, so a structural mechanism is not needed to mediate different cell fates. In other words, one stem cell daughter in the female produces one egg, and in the male, one stem cell daughter produces 64 sperm. Perhaps removal of the female fusome is necessary to ensure the production of one egg per stem cell division. While there is evidence that male fusomes participate in mitotic spindle alignment (Miyauchi et al., 2013), we can now conclude that fusomes are not essential for either mitosis or meiosis during spermatogenesis, at least under normal conditions. They may, however, have a role in responding to abnormal conditions, as seen in the presence of DNA damage in 16-cell spermatogonial cysts (Lu & Yamashita, 2017).

Our live imaging data support a function for RCs during spermatogenesis in mediating cytoplasmic content sharing between the cells in a cyst; however, more could be learned about RC function through their targeted disruption or occlusion. Our attempts at RC disruption have focused on RNAi of RC proteins, but these efforts led to cytokinesis defects rather than a RC-specific phenotype. To progress, new tools must be developed to disrupt RC function *in vivo*, perhaps by occlusion or targeted disruption, to study the functional consequences of RC loss during spermatogenesis. Disruption of the RCs in this manner could provide additional evidence for RC involvement in cell-cycle synchronization, maintenance of overall cyst health, and sharing of post-meiotic gene products.

Materials and Methods

Drosophila strains

The following Drosophila lines were generously provided by the referenced authors: 20XUAS- mC3PA-GFP and 10XUAS-GFP (Pfeiffer et al., 2012), *bam-Gal4* (Chen & McKearin, 2003), *hts*[1](Yue & Spradling, 1992), *hts*[W532X] (gift from Trudy Schüpbach), and *hts*[ΔG] (Koundakjian et al., 2004). The following FlyTrap lines were used: GFP::CaM (YC0069LE), eIF4A::GFP (YC0001), and GFP::Oda (YD0523) (Buszczak et al., 2007; Lowe et al., 2014; Nagarkar-Jaiswal et al., 2015; Quiñones-Coello et al., 2007). *nos-Gal4* (stock #7303), αSpectrin shRNA (stock #56932), *hts*[1103] (stock#10989), *hts* shRNA (stock #35421), Df(2R)BSC135/CyO (stock #9423), GFP::Clu (stock #6842), GFP::eIF4E1 (stock #50858), GFP::CG32701 (stock #50839), GFP::Lost (stock #6832), Mito::GFP (stock #8442), Pdcd4::GFP (stock #38446), GFP::Sgg (stock #50887), GFP::Kra (stock #50873), GFP::Men-B (stock #50854), and GFP::βTub56D (stock #50867) were obtained from the Bloomington Drosophila Stock Center. All animals were raised at room temperature or in a 25°C incubator.

Construction of transgenes and generation of transgenic lines

To visualize RC components at endogenous levels, we recombineered GFP into a BAC containing the Pavarotti (Pav) gene at the C-terminus (BAC ID 322-102N3) to create Pav::GFP. This BAC contains the entire *pav* locus on a 21 kb genomic fragment (chr3L:4,229,286...4,250,505, FlyBase release 6). Briefly, we used a 2-step BAC recombineering protocol to first insert a Kanamycin resistance cassette (Wang et al., 2006) that was subsequently replaced by HA::GFP::FLAG through streptomycin selection. The final plasmid was injected into BL#24872 into the attP-3B site on chr2L at Rainbow Transgenic Flies, Inc. (Camarillo, CA).

Immunocytochemistry

Testes were dissected in IMADS buffer (ionically matched Drosophila saline) (Singleton & Woodruff, 1994) and fixed for 10 min in 4% paraformaldehyde in PBT (phosphate-buffered saline with 0.3% Triton X-100 and 0.5% BSA). Fixed tissue was washed in PBT and incubated with anti-Hts1B1 (1:50, Developmental Studies Hybridoma Bank (DSHB), (Zaccai & Lipshitz, 1996) or anti-αSpec 3A9 (1:50, DSHB (Dubreuil et al., 1987)). Secondary antibodies used were goat anti-mouse conjugated to Alexa-568 (1:500, Invitrogen). Samples were washed in PBT and mounted on slides in Aqua PolyMount (Polysciences, Inc.). Samples were imaged with a Leica SP8 confocal microscope and a 40X 1.3 NA oil-immersion objective lens and analyzed as maximum Z-projections.

Photoactivation of PA-GFP

Live testes expressing Pav::GFP and PA-GFP with or without *αSpec* shRNA driven by a *nos-Gal4* or *bam-Gal4* driver were dissected in a small drop of IMADS on a coverslip. Testes were gently scored to release both spermatogonia and spermatocytes and break the muscle to prevent muscle contraction and prevent the testes from shifting during imaging. A slide was placed over the coverslip squashing the testes and extra buffer was wicked away using a Kimwipe. The slide was sealed with VALAP (equal parts vaseline, lanolin, and paraffin) and imaged within 15 minutes. Photoactivation and subsequent live imaging of PA-GFP was accomplished on an inverted Leica SP8 confocal microscope and a 40X 1.3 NA oil-immersion objective lens using the FRAP mode. Photoactivation was accomplished with 30 scan iterations of 405 nm light over regions of interest. Activated GFP was observed by capturing a single z-slice using 488 nm excitation every 30 seconds for ~10 minutes.

Male fertility assay

Fertility of the fusome-less males was assessed by pairing a single male with three CantonS or w^{1118} virgin females. These males were shifted to new vials with fresh females every two days for 14 days and the total number of adult progeny was counted to determine fertility.

Transmission electron microscopy

For analysis by EM, ~20 testis samples were fixed in 2.5% gluteraldehyde and 2% paraformaldehyde in 0.1M sodium cacodylate buffer pH 7.4 for 30 minutes at room temperature followed by 1 hour at 4°C. The samples were rinsed in buffer then post-fixed in 1% osmium tetroxide and en bloc stained in 2% aqueous uranyl acetate for one hour. Tissue was rinsed and dehydrated in an ethanol series followed by epon resin (Embed812 Electron Microscopy Science) infiltration, oriented, and baked overnight at 60°C. Hardened blocks were cut using a Leica UltraCut UCT. 60 nm sections were collected on formvar/carbon coated grids and contrast stained using 2% uranyl acetate and lead citrate. Samples were viewed using FEI Tencai Biotwin TEM at 80Kv. Images were taken using a Morada CCD and iTEM (Olympus) software.

Fluorescence Loss in Photobleaching (FLIP)

FLIP of UAS-GFP and all GFP-traps was conducted using a Leica SP8 microscope. 16- or 64-cell cysts were dissected out of the testis in a manner as described above. Microscope pinhole size was set to 7 to generate visible bleaching of GFP using the following sequence: [1 pre-bleach, 30 iterations of bleaching, 1 post-bleach] x 48 for 1 hour of imaging while repositioning the sample as necessary to account for drift. GFP bleaching and single z-slice image capture was performed using a 488 nm laser. All images were processed using FIJI. To quantify fluorescence loss, an ROI was drawn around the entire bleached area of a cyst and the mean pixel intensity for this region was measured for the duration of the movie using Time Series Analyzer (FIJI). Similarly, an ROI was drawn around the remainder of the cyst, outside of the bleached region, and the mean pixel intensities were measured. These values were plotted against the mean pixel values from an ROI of similar size in a neighboring control cell to control for loss of signal due to generalized photobleaching. Raw values of the mean pixel intensities were exported into GraphPad Prism to generate representative graphs of each GFP protein.

Quantification of Fusome Knockdown

Knockdown of the fusome was quantitatively assessed from electron micrographs of control (Pav::GFP, w^{1118} or *nos-Gal4;* n=12) and *nos>αSpec RNAi* (n=12) testes. Three non-overlapping ROIs of 40 μm^2 were assigned to the RC lumen between or immediately adjacent to the electron dense plasma membrane. Similarly, three non-overlapping ROIs of 40 μm^2 were assigned to measure the cytoplasm distant from the RC lumen. From the resulting histograms, the standard deviation was measured and used as a proxy for ribosome density. The standard deviations from each cytoplasmic compartment (RC or non-RC) were averaged to account for differences in staining across preparations. Measurements were exported into R Studio for further analysis and data visualization. Statistical significance was determined by a two-tailed Student's t-test.

Quantitative Analysis of GFP Movement

Movement of GFP fluorescence, both in PA-GFP and FLIP experiments, was assessed by recording fluorescence intensities in experimental and non-activated control cells over the course of the movies. Average pixel intensity values from a 1256 pixel^2 region of interest (ROI) in the cytoplasm of either the donor or acceptor cell(s) were measured using the Time Series Analyzer in FIJI. In cysts with more than one acceptor cell, all cells in the focal plane were averaged to generate a single trace. Fluorescence values were normalized by subtracting the average fluorescence intensity of an ROI of the same size from two adjacent, non-photoactivated cells. Measurements were exported into Excel for further analysis and GraphPad Prism for data visualization.

Measurements of GFP movement in elongated spermatids were acquired using the Time Series Analyzer in FIJI. Six 1256 pixel^2 ROIs were assigned as described in Figure 4M and the mean pixel values of each ROI were plotted as a function of time. Raw values were exported into Excel for further analysis and GraphPad Prism for data visualization. A total of three spermatid bundles were analyzed and plotted individually because of differing levels of GFP fluorescence.

To quantitatively assess rates of movement of PA-GFP between cells in wild-type and fusome knockdown testes, a Bruker Opterra II Swept Field Microscope was used, with a 60X water immersion objective lens. Wild-type (w^{1118}) and *bam>αSpec RNAi* testes were scored and mounted as described above. PA-GFP was activated by a single iteration of 405 nm light in one z-plane and movies were captured in a 15-20 slice z-stack encompassing the cyst every 10 seconds for a total of 10 minutes. Maximum intensity projections were generated in FIJI, and the total fluorescence of PA-GFP in the activated and recipient cell was measured at each time point. For comparison purposes, we only quantified movies in which PA-GFP was activated within a single spermatocyte cell and diffused into one other recipient cell. We note that although the cells imaged in these experiments were from 16-cell cysts, PA-GFP diffusion usually was restricted to 1-5 other cells indicating that the tissue-scoring preparation used may have caused cell clusters to become dissociated from the rest of the cyst. The PA-GFP relative fluorescence units (RFU) between the activated and the recipient cells were summed and normalized to 1. The mean RFU of PA-GFP in the recipient cell (as a fraction of total RFU

between the two cells) for wild-type and fusome knockdown conditions was plotted over time (n=9 for wild-type; n=11 for fusome knockdown). A nonlinear regression was used to fit the data to a one phase exponential association model using the following equation:

$$Y = Y_0 + (Plateau - Y_0) * (1 - e^{(-K*x)})$$

The best-fit curve was plotted alongside the mean RFU data points for each condition (see Figure S12). Comparison of fits was performed to check for statistically significant differences in the best-fit values between wild-type and fusome knockdown fits.

Acknowledgments

Author Contributions

Conceptualization: R.S.K., L.C.; Investigation: R.S.K., K.L.P., K.M.M., K.M.A., A.M.H., L.C., Writing - Original Draft: R.S.K.; Writing - Review & Editing: R.S.K., K.L.P., K.M.M., K.M.A., A.M.H., L.C.; Visualization: R.S.K., K.L.P., K.M.M.; Funding Acquisition: L.C.; Resources: R.S.K., K.L.P., K.M.M., K.M.A., A.M.H., L.C.; Supervision: L.C.

Declaration of Interests

These authors have no competing interests.

References

Airoldi, S. J., McLean, P. F., Shimada, Y. and Cooley, L. (2011). Intercellular protein movement in syncytial Drosophila follicle cells. *J. Cell Sci.* 124, 4077–4086.

Barreau, C., Benson, E., Gudmannsdottir, E., Newton, F. and White-Cooper, H. (2008). Post-meiotic transcription in Drosophila testes. *Development* 135, 1897–1902.

Barreau, C., Benson, E. and White-Cooper, H. (2008). Comet and cup genes in Drosophila spermatogenesis: The first demonstration of post-meiotic transcription. *Biochem. Soc. Trans.* 36, 540–542.

Braun, R. E., Behringer, R. R., Peschon, J. J., Brinster, R. L. and Palmiter, R. D. (1989). Genetically haploid spermatids are phenotypically diploid. *Nature* 337, 373–376.

Brown, R. K. and Smith, W. L. (1964). Chromosomal studies in ovarian dysgenesis. *Trans. N. Engl. Obstet. Gynecol. Soc.* 18, 47–54.

Burgos, M. H. and Fawcett, D. W. (1955). Studies on the fine structure of the mammalian testis. I. Differentiation of the spermatids in the cat (Felis domestica). *J. Biophys. Biochem. Cytol.* 1, 287–300.

Buszczak, M., Paterno, S., Lighthouse, D., Bachman, J., Planck, J., Owen, S., Skora, A. D., Nystul, T. G., Ohlstein, B., Allen, A., et al. (2007). The carnegie protein trap library: A versatile tool for drosophila developmental studies. *Genetics* 175, 1505–1531.

Chen, D. and McKearin, D. M. (2003). A discrete transcriptional silencer in the bam gene determines asymmetric division of the Drosophila germline stem cell. *Development* 130, 1159–1170.

De Cuevas, M., Lilly, M. and Spradling, A. (1997). Germline Cyst Formation in Drosophila. *Annu. Rev. Genet.* 31, 405–428.

De Cuevas, M., Lee, J. K. and Spradling, A. C. (1996). α-spectrin is required for germline cell division and differentiation in the Drosophila ovary. *Development* 122, 3959–3968.

De Cuevas, M. and Spradling, A. C. (1998). Morphogenesis of the Drosophila fusome and its implications for oocyte specification. *Development* 125, 2781–2789.

Deng, W. and Lin, H. (1997). Spectrosomes and fusomes anchor mitotic spindles during asymmetric germ cell divisions and facilitate the formation of a polarized microtubule array for oocyte specification in Drosophila. *Dev. Biol.* 189, 79–94.

Dubreuil, R., Byers, T. J., Branton, D., Goldstein, L. S. and Kiehart, D. P. (1987). Drosophilia spectrin. I. Characterization of the purified protein. *J. Cell Biol.* 105, 2095–2102.

Dym, M. and Fawcett, D. W. (1971). Further Observations on the Numbers of Spermatogonia, Spermatocytes, and Spermatids Connected by Intercellular Bridges in the Mammalian Testis. *Biol. Reprod.* 4, 195–215.

Fabrizio, J. J., Hime, G., Lemmon, S. K. and Bazinet, C. (1998). Genetic dissection of sperm individualization in Drosophila melanogaster. *Development* 125, 1833–1843.

Fawcett, D. W., Ito, S. and Slautterback, D. (1959). The occurrence of intercellular bridges in groups of cells exhibiting synchronous differentiation. *J. Biophys. Biochem. Cytol.* 5, 453–460.

Fuller, M. T. (1993). *The Development of Drosophila melanogaster*. 1st ed. (ed. Bate, M. and Martinez Arias, A.) Plainview, New York: Cold Spring Harbor Laboratory Press.

Gärthner, S. M. K., Rathke, C., Renkawitz-Pohl, R. and Awe, S. (2014). *Ex vivo* culture of Drosophila pupal testis and single male germ-line cysts: Dissection, imaging, and pharmacological treatment. *J. Vis. Exp.* 91, e51868.

Greenbaum, M. P., Iwamori, T., Buchold, G. M. and Matzuk, M. M. (2011). Germ cell intercellular bridges. *Cold Spring Harb. Perspect. Biol.* 3, 1–18.

Grieder, N. C., de Cuevas, M. and Spradling, A. C. (2000). The fusome organizes the microtubule network during oocyte differentiation in Drosophila. *Development* 127, 4253-4264.

Haglund, K., Nezis, I. P. and Stenmark, H. (2011). Structure and functions of stable intercellular bridges formed by incomplete cytokinesis during development. *Commun. Integr. Biol.* 4, 1–9.

Hime, G. R., Brill, J. A. and Fuller, M. T. (1996). Assembly of ring canals in the male germ line from structural components of the contractile ring. *J. Cell Sci.* 109, 2779–2788.

Huckins, C. and Oakberg, E. F. (1978). Morphological and quantitative analysis of spermatogonia in mouse testes using whole mounted seminiferous tubules. II. The irradiated testes. *Anat. Rec.* 192, 529–541.

Huynh, J. R. and St Johnston, D. (2004). The origin of asymmetry: Early polarisation of the Drosophila germline cyst and oocyte. *Curr. Biol.* 14, 438–449.

Jandura, A., Hu, J., Wilk, R. and Krause, H. M. (2017). High resolution fluorescent in situ hybridization in Drosophila embryos and tissues using tyramide signal amplification. *J. Vis. Exp.* 2017, e56281.

Koch, E. A. and King, R. C. (1966). The origin and early differentiation of the egg chamber of Drosophila melanogaster. *J. Morphol.* 119, 283–303.

Koch, E. A. and King, R. C. (1969). Further studies on the ring canal system of the ovarian cystocytes of Drosophila melanogaster. *Zeitschrift für Zellforsch. und Mikroskopische Anat.* 102, 129–152.

Koundakjian, E. J., Cowan, D. M., Hardy, R. W. and Becker, A. H. (2004). The Zuker collection: A resource for the analysis of autosomal gene function in Drosophila melanogaster. *Genetics* 167, 203–206.

León, A. and McKearin, D. (1999). Identification of TER94, an AAA ATPase protein, as a Bam-dependent component of the Drosophila fusome. *Mol. Biol. Cell* 10, 3825–3834.

Lighthouse, D. V., Buszczak, M. and Spradling, A. C. (2008). New components of the Drosophila fusome suggest it plays novel roles in signaling and transport. *Dev. Biol.* 317, 59–71.

Lilly, M. A., De Cuevas, M. and Spradling, A. C. (2000). Cyclin A associates with the fusome during germline cyst formation in the Drosophila ovary. *Dev. Biol.* 218, 53–63.

Lin, H. and Spradling, A. C. (1995). Fusome asymmetry and oocyte determination in Drosophila. *Dev. Genet.* 16, 6–12.

Lin, H., Yue, L. and Spradling, A. C. (1994). The Drosophila fusome, a germline-specific organelle, contains membrane skeletal proteins and functions in cyst formation. *Development* 120, 947–956.

Lowe, N., Rees, J. S., Roote, J., Ryder, E., Armean, I. M., Johnson, G., Drummond, E., Spriggs, H., Drummond, J., Magbanua, J. P., et al. (2014). Analysis of the expression patterns, Subcellular localisations and interaction partners of Drosophila proteins using a pigP protein trap library. *Development* 141, 3994–4005.

Lu, K. L. and Yamashita, Y. M. (2017). Germ cell connectivity enhances cell death in response to DNA damage in the Drosophila testis. *Elife* 6, e27960.

Lu, K., Jensen, L., Lei, L. and Yamashita, Y. M. (2017). Stay Connected: A Germ Cell Strategy. *Trends Genet.* 33, 971–978.

McGrail, M. and Hays, T. S. (1997). The microtubule motor cytoplasmic dynein is required for spindle orientation during germline cell divisions and oocyte differentiation in Drosophila. *Development* 124, 2409–2419.

McKearin, D. and Ohlstein, B. (1995). A role for the Drosophila Bag-of-marbles protein in the differentiation of cystoblasts from germline stem cells. *Development* 121, 2937–2947.

McLean, P. F. and Cooley, L. (2013). Protein equilibration through somatic ring canals in Drosophila. *Science* 340, 1444–1447.

Miyauchi, C., Kitazawa, D., Ando, I., Hayashi, D. and Inoue, Y. H. (2013). Orbit/CLASP Is Required for Germline Cyst Formation through Its Developmental Control of Fusomes and Ring Canals in Drosophila Males. *PLoS One* 8, e58220.

Morales, C. R., Lefrancois, S., Chennathukuzhi, V., El-Alfy, M., Wu, X., Yang, J., Gerton, G. L. and Hecht, N. B. (2002). A TB-RBP and Ter ATPase complex accompanies specific mRNAs from nuclei through the nuclear pores and into intercellular bridges in mouse male germ cells. *Dev. Biol.* 246, 480–494.

Nagarkar-Jaiswal, S., Lee, P. T., Campbell, M. E., Chen, K., Anguiano-Zarate, S., Gutierrez, M. C., Busby, T., Lin, W. W., He, Y., Schulze, K. L., et al. (2015). A library of MiMICs allows tagging of genes and reversible, spatial and temporal knockdown of proteins in Drosophila. *Elife* 2015, e05338.

Pfeiffer, B. D., Truman, J. W. and Rubin, G. M. (2012). Using translational enhancers to increase transgene expression in Drosophila. *Proc. Natl. Acad. Sci. U. S. A.* 109, 6626–6631.

Quiñones-Coello, A. T., Petrella, L. N., Ayers, K., Melillo, A., Mazzalupo, S., Hudson, A. M., Wang, S., Castiblanco, C., Buszczak, M., Hoskins, R. A., et al. (2007). Exploring strategies for protein trapping in Drosophila. *Genetics* 175, 1089–1104.

Ren, H. P. and Russell, L. D. (1991). Clonal development of interconnected germ cells in the rat and its relationship to the segmental and subsegmental organization of spermatogenesis. *Am. J. Anat.* 192, 121–128.

Robinson, D. and Cooley, L. (1996). Stable intercellular bridges in development: the cytoskeleton lining the tunnel. *Trends Cell Biol.* 6, 474–479.

Röper, K. (2007). Rtnl1 is enriched in a specialized germline ER that associates with ribonucleoprotein granule components. *J. Cell Sci.* 120, 1081–1092.

Sanabria, H., Digman, M. A., Gratton, E. and Waxham, M. N. (2008). Spatial diffusivity and availability of intracellular calmodulin. *Biophys. J.* 95, 6002–6015.

Singleton, K. and Woodruff, R. I. (1994). The osmolarity of adult Drosophila hemolymph and its effect on oocyte-nurse cell electrical polarity. *Dev. Biol.* 161, 154–167.

Snapp, E. L., Iida, T., Frescas, D., Lippincott-Schwartz, J. and Lilly, M. A. (2004). The fusome mediates intercellular endoplasmic reticulum connectivity in Drosophila ovarian cysts. *Mol. Biol. Cell* 15, 4512–4521.

Theurkauf, W. E., Alberts, B. M., Jan, Y. N. and Jongens, T. A. (1993). A central role for microtubules in the differentiation of Drosophila oocytes. *Development* 118, 1169–1180.

Tokuyasu, K. T., Peacock, W. J. and Hardy, R. W. (1972). Dynamics of spermiogenesis in Drosophila melanogaster. I. Individualization process. *Z. Zellforsch. Mikrosk. Anat.* 124, 479–506.

Wang, J., Sarov, M., Rientjes, J., Fu, J., Hollak, H., Kranz, H., Xie, W., Stewart, A. F. and Zhang, Y. (2006). An improved recombineering approach by adding RecA to λ red recombination. *Mol. Biotechnol.* 32, 43–53.

White-Cooper, H. (2010). Molecular mechanisms of gene regulation during Drosophila spermatogenesis. *Reproduction* 139, 11–21.

Wilson, P. G. (2005). Centrosome inheritance in the male germ line of Drosophila requires *hu-li tai-shao* function. *Cell Biol. Int.* 29, 360–369.

Yamashita, Y. M. (2018). Subcellular specialization and organelle behavior in germ cells. *Genetics* 208, 19–51.

Yan, D., Neumüller, R. A., Buckner, M., Ayers, K., Li, H., Hu, Y., Yang-Zhou, D., Pan, L., Wang, X., Kelley, C., et al. (2014). A regulatory network of Drosophila germline stem cell self-renewal. *Dev. Cell* 28, 459–473.

Yue, L. and Spradling, A. C. (1992). *hu-li tai shao,* a gene required for ring canal formation during Drosophila oogenesis, encodes a homolog of adducin. *Genes Dev.* 6, 2443–2454.

Zaccai, M. and Lipshitz, H. D. (1996). Differential distributions of two adducin-like protein isoforms in the Drosophila ovary and early embryo. *Zygote* 4, 159–166.
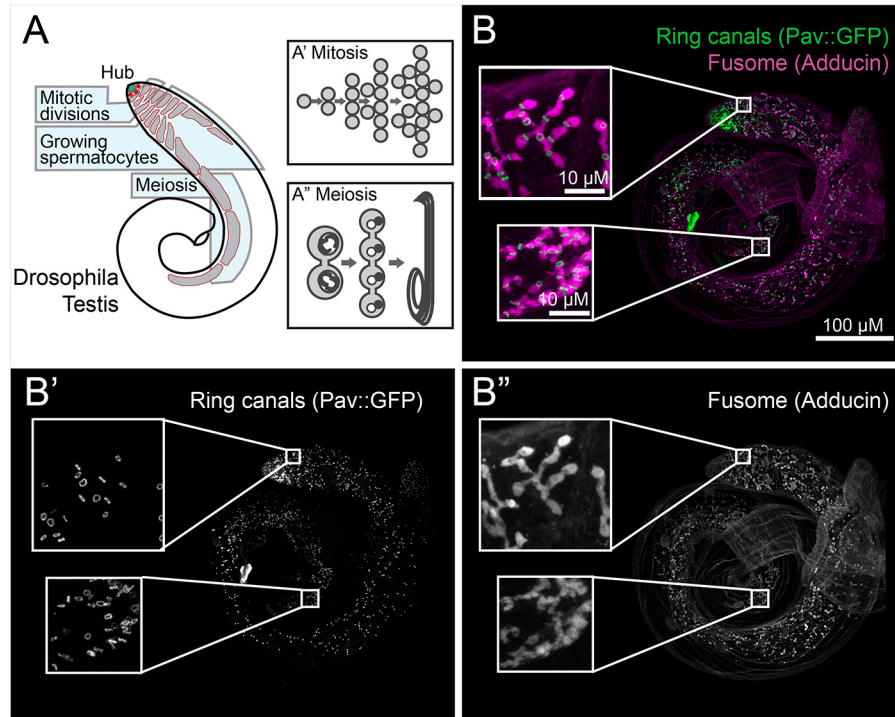
Figure 1. Overview of spermatogenesis in the Drosophila testis. (A) Cartoon depicting spermatid development in Drosophila. Germline stem cells (red) are located at the hub (green) of the testis. (A') Spermatogonia divide mitotically four times to form a 16-cell cyst. (A") These cysts undergo a growth phase of ~3 days before undergoing two rounds of meiosis to form 64-cell cysts. Following this, each cell elongates a tail to form bundles of mature spermatids. (B-B") Immunofluorescence shows that ring canals marked by Pav::GFP (B') and the fusome stained with Adducin antibody (B") are present throughout spermatogenesis.
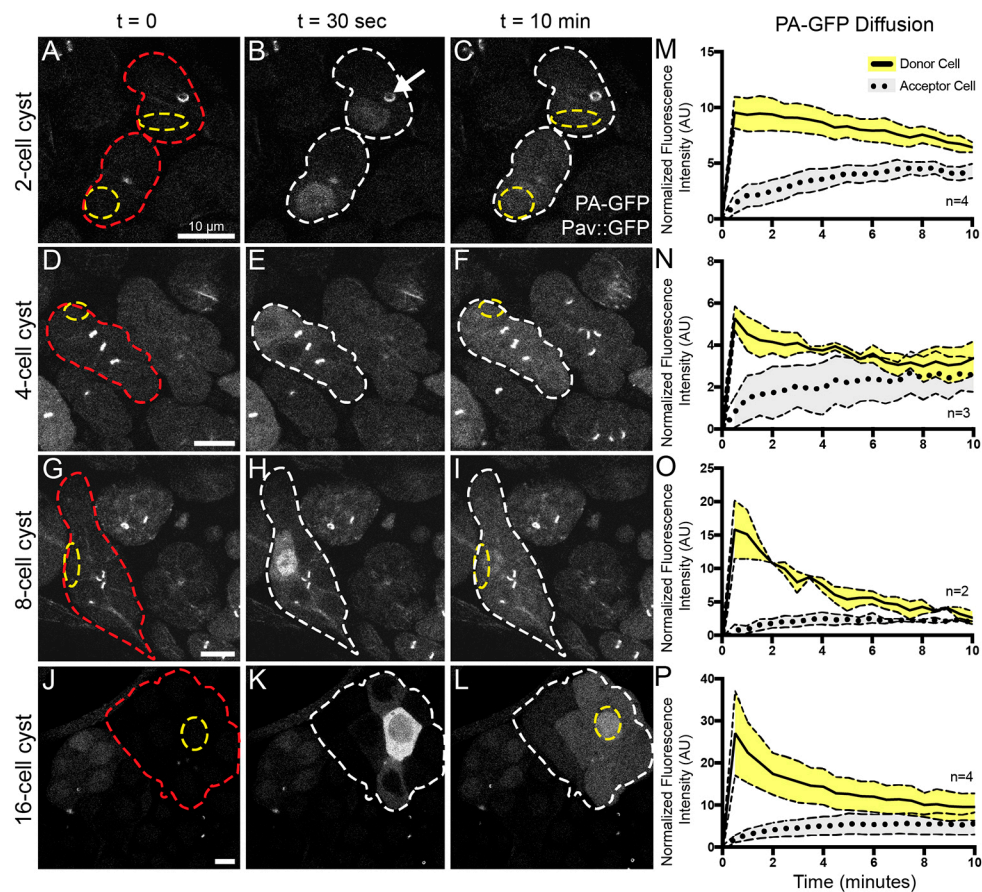
Figure 2. RCs allow movement of GFP between germline cells in a cyst. (A-L) Live imaging of activated PA-GFP at various stages of spermatogenesis reveals sharing of GFP between cells in a cyst (red outline) through the ring canals (marked with Pav::GFP, white arrow). After activation of PA-GFP in a single cell or small region of cells (yellow outline), GFP was found in most of the cells in that cyst after 10 minutes (white outline). (M-P) Quantification of PA-GFP movement following photoactivation from a single donor cell (solid line) to other cells within the cyst (dashed line represents the fluorescence intensity from an average of all other non-activated cells within the same cyst). Normalized fluorescence intensity (AU) was plotted with respect to time. Error bars represent SEM.
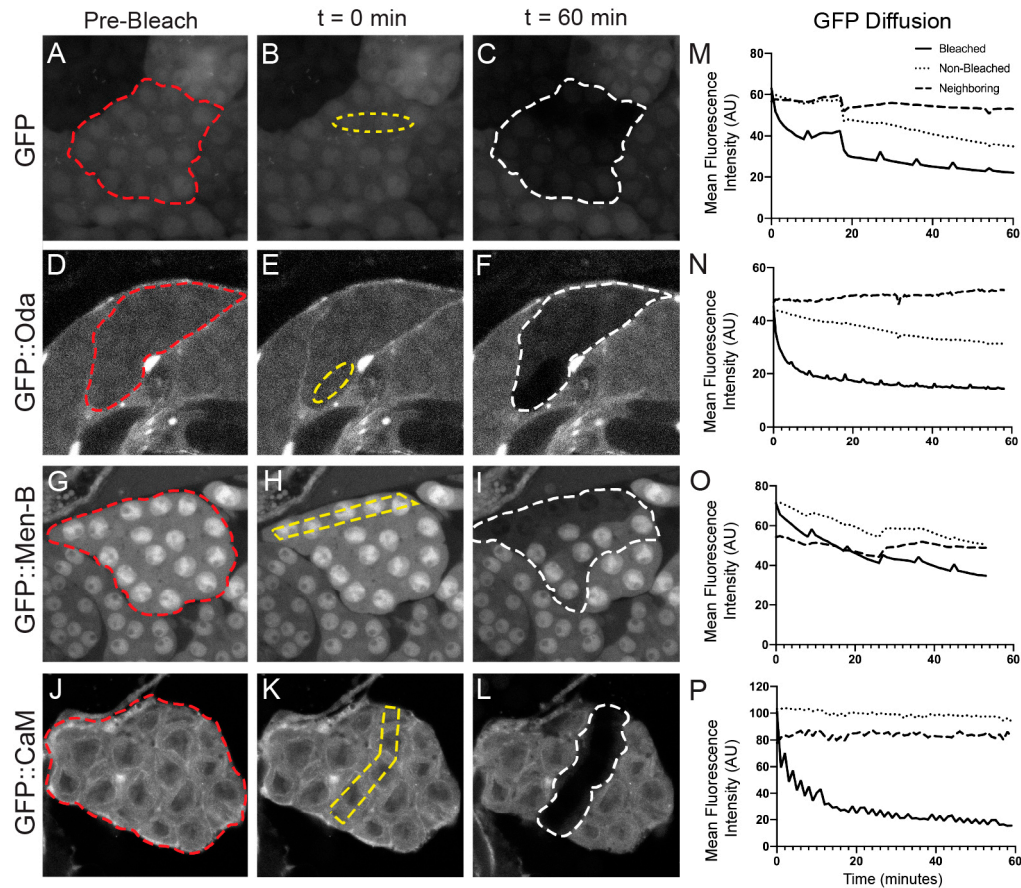
Figure 3. RCs allow for sharing of some, but not all, proteins. (A-L) Fluorescence Loss in Photobleaching (FLIP) demonstrated that not all GFP-tagged proteins move between the cells in a 16-cell cyst. Several cells within a 16-cell cyst (red outline) expressing GFP or a GFP-tagged protein were continuously bleached (yellow outline) over the course of 1 hour. Protein movement was determined by a loss in GFP fluorescence from neighboring cells within that cyst (white outline) indicating that GFP from non-bleached cells moved into the bleached region. (M-P) Quantification of GFP from the representative images (A-L) in the bleached (solid line), non-bleached (dotted line), and neighboring (dashed line) regions in a spermatocyte cyst. FLIP was detected for GFP, GFP::Oda, GFP::Men-B but not GFP::CaM. Mean fluorescence intensity (AU) is plotted with respect to time. Intermittent peaks on the graphs represent quick recovery of GFP in the sample while the microscope switches between capture and bleach modes.
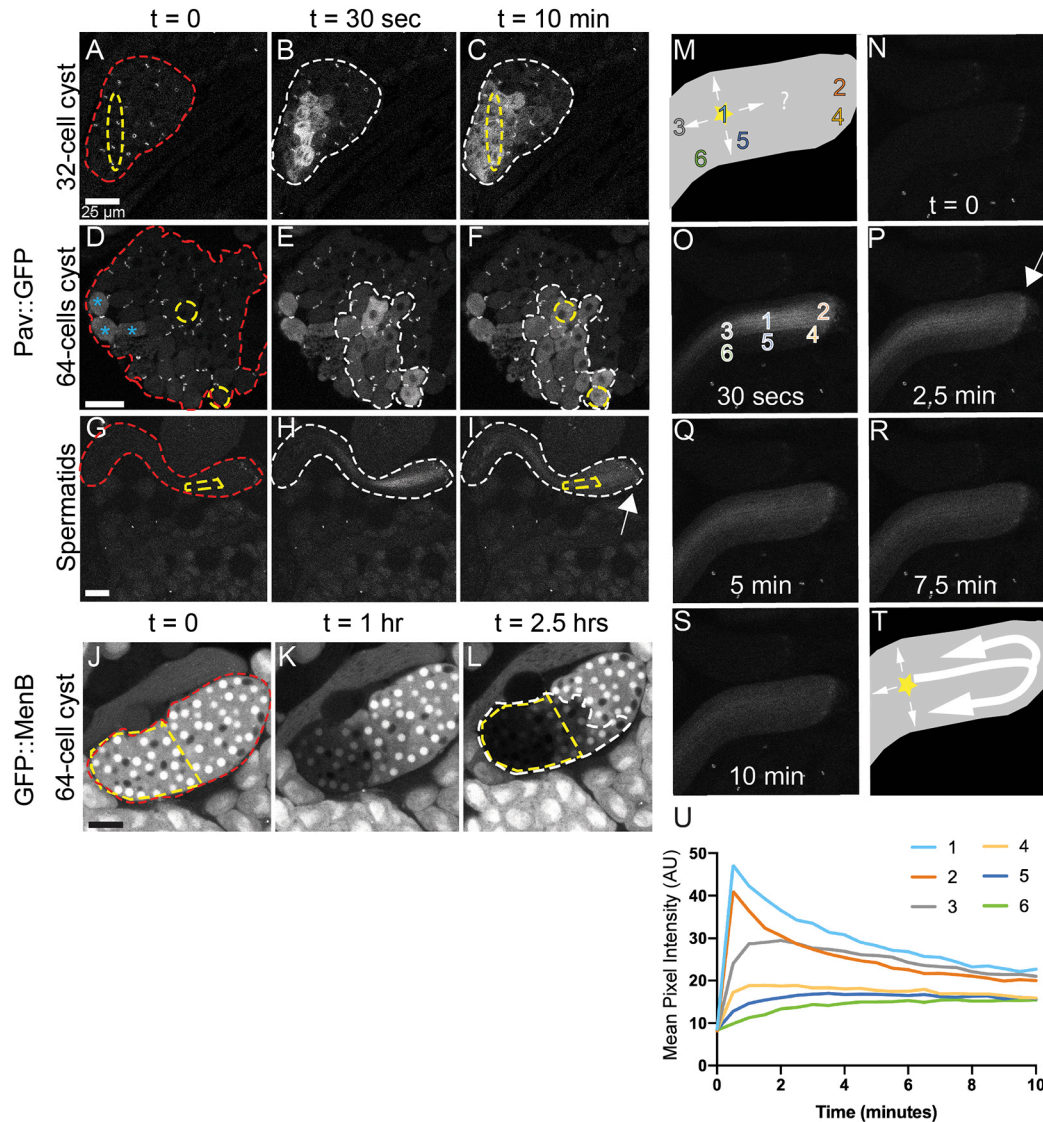
Figure 4. Movement of proteins in meiotic cysts and haploid spermatids. (A-I) After meiosis I and II, and during elongation of spermatid tails, PA-GFP moved between cells of a cyst (red outline). PA-GFP activated within a small region of the cyst (yellow outline) appeared in neighboring cells within that cyst (white outline). Cells activated previously in (D) are marked with blue asterisks. White arrow marks RC end of spermatid bundle. (J-L) Movement of endogenous GFP::Men-B occurred in post-meiotic 64-cell cysts. Bleaching zone in this FLIP experiment is outlined in yellow. Cells with loss of fluorescence are outlined in white. (M) Cartoon of spermatid bundle depicting possible pathways of PA-GFP spread after activation (marked by star at position 1). (N-S) PA-GFP activation in a spermatid bundle over the course of 10 minutes with activation occurring in region 1 (shown in panel O). (T) Cartoon of actual PA-GFP spread showing that movement is predominantly through RCs rather than through lateral perforations. (U) Normalized fluorescence intensity of PA-GFP over time measured at the regions indicated in (O). GFP fluorescence increased in region 4 (yellow line) before region 5 (dark blue line). RC end of spermatid bundles marked by arrow.
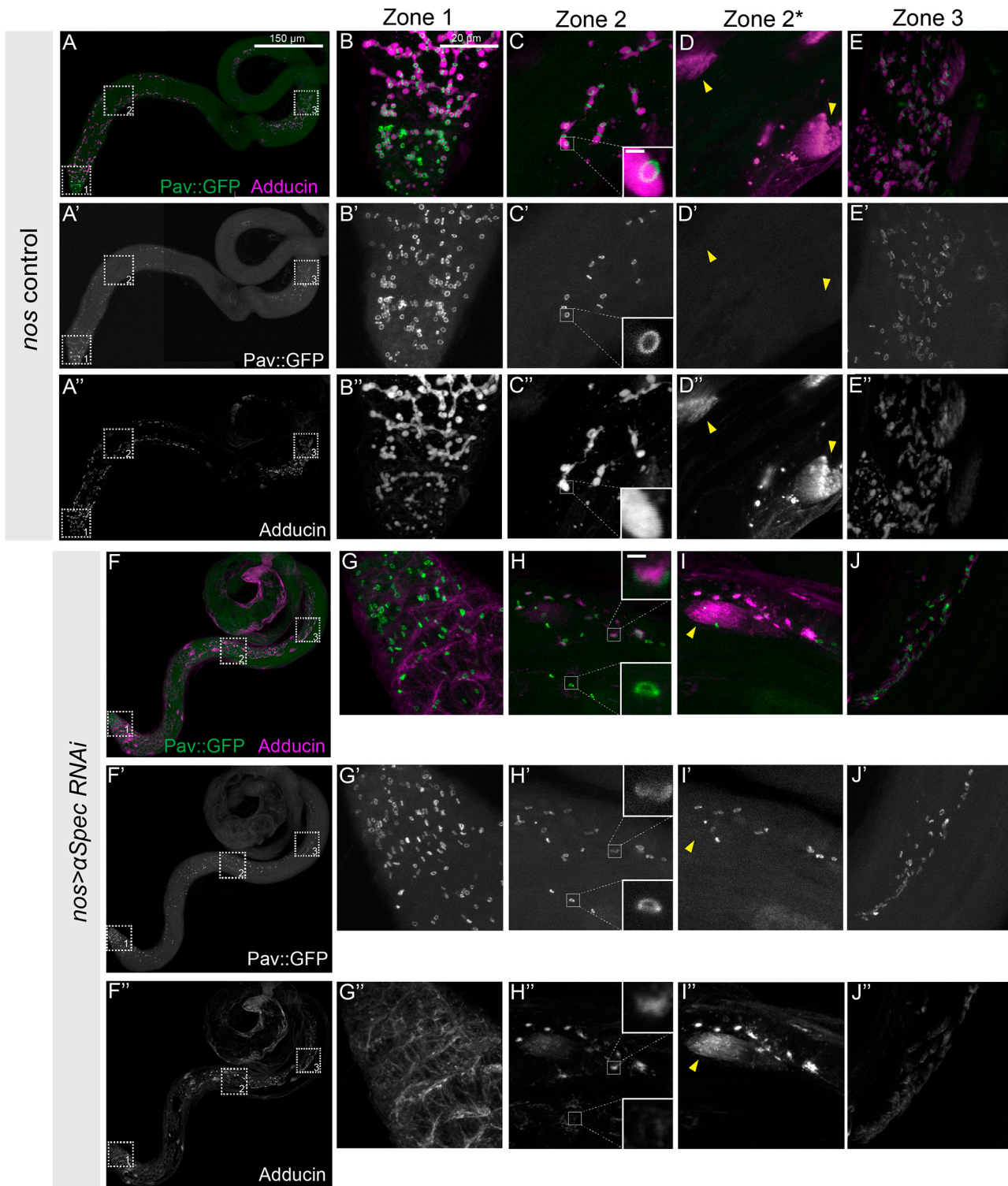
Figure 5. *nos Gal4*-driven knockdown of *α*Spectrin is sufficient to compromise the fusome throughout spermatogenesis. (A) Wild-type testis with RCs marked by Pav::GFP and fusomes labeled with Adducin antibody (1B1). (B-E) Closeups of the regions marked by box in (A), highlighting the RCs (Pav, green) and fusome (Adducin, purple) in a wild-type testis in three different stages of development: mitotic (Zone 1), post-mitotic (Zone 2), and elongated spermatids (Zone 3). Insets in (C-C") highlight one RC, scale bar is 1 μm. (D, I) Zone 2* highlights the growing ends of spermatid tails from the same ROI, but different Z plane, as Zone 2. (F) Testes with α*Spec RNAi* driven by *nos-Gal4* lack Adducin staining at the fusome, but testis morphology appears unaffected. (F-J) Closeups of the regions marked in (F) showing Adducin staining at the membrane rather than in a fusome pattern, while Pav::GFP remained localized to the RCs.
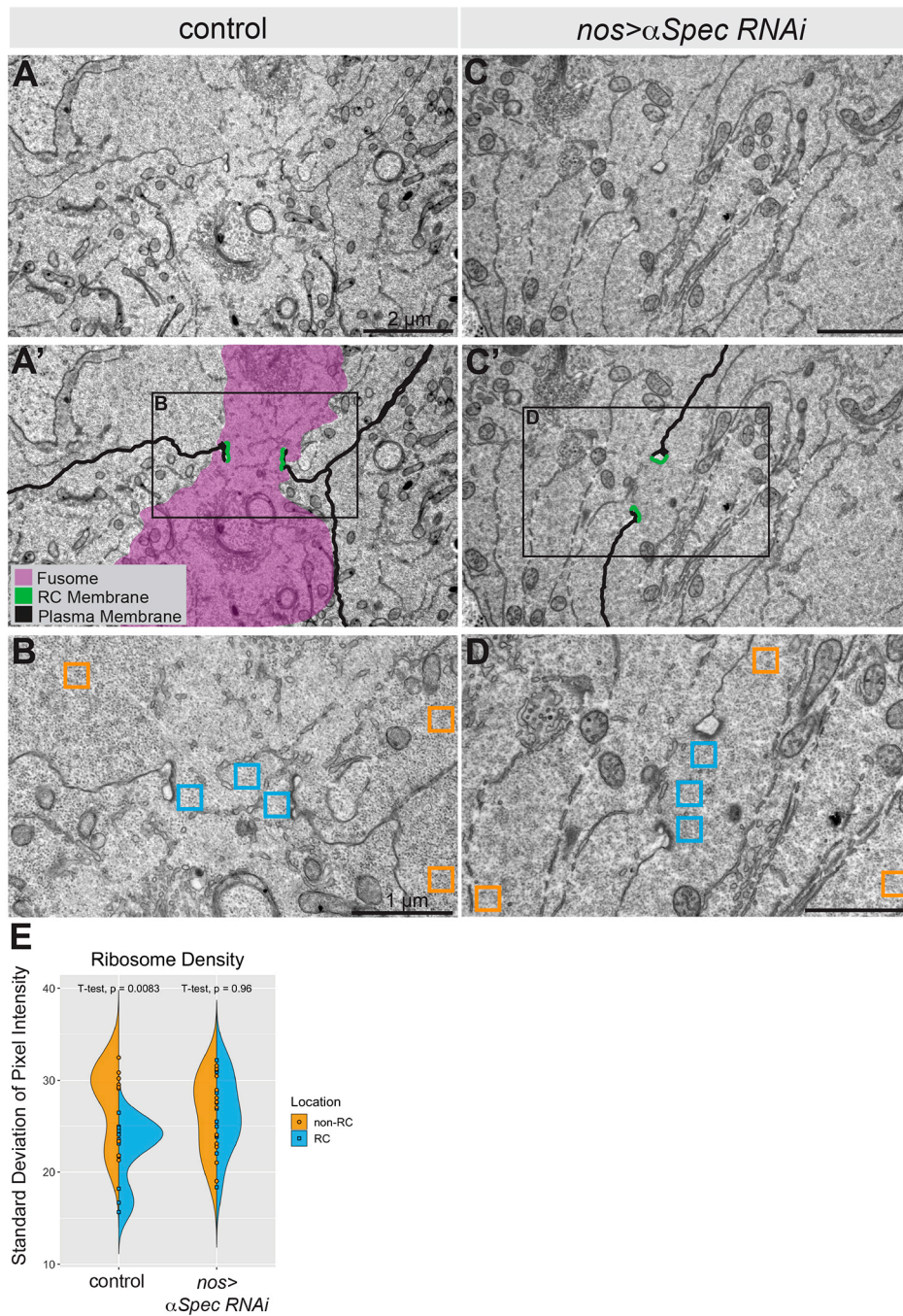
Figure 6. Ribosome density reveals lack of fusome in α*Spectrin RNAi* testes. (A) EM of Pav::GFP testis revealed electron dense RCs surrounding a fusome. (A') False coloring of (A) highlights electron dense RCs (green), plasma membrane (black), and a ribosome-free fusome area (purple). (B) Inset marked in (A') shows locations used for quantification of ribosome density in (E). (C) EM of two cells connected by a RC in a α*Spec* RNAi testis. (C') False coloring of (C) highlighting RCs (green) and a plasma membrane (black) but no discernable fusome structure. (D) Inset marked in (C') shows locations used for quantification of ribosome density in (E) in the α*Spec RNAi* testis.
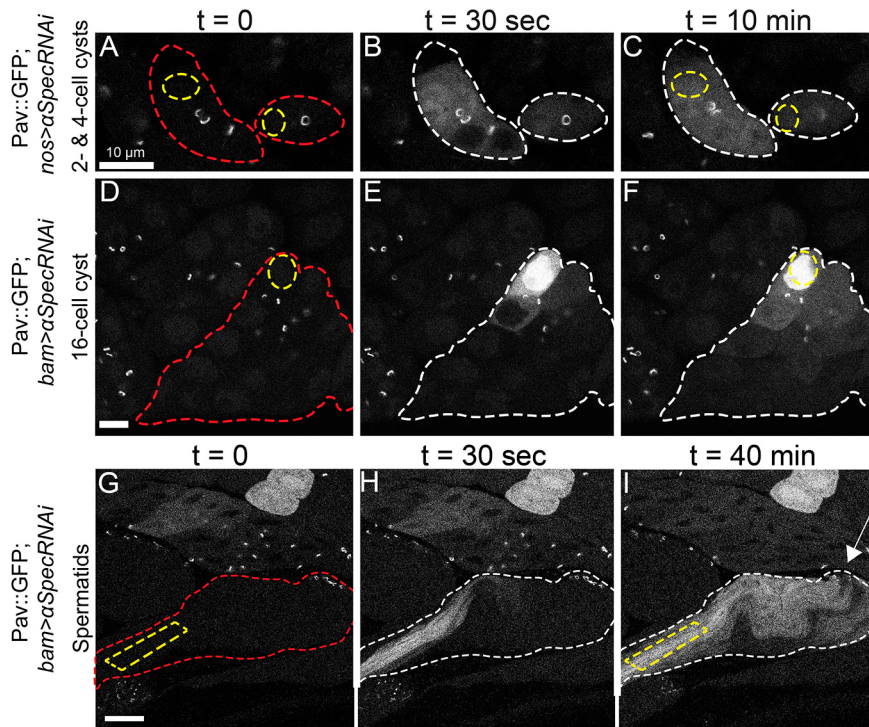
Figure 7. PA-GFP moves through RCs despite knockdown of fusome components. *αSpec RNAi* driven by *nos-Gal4* in 2- and 4-cell spermatogonia (A-C) and *bam-Gal4* in 16-cell spermatocyte cysts (D-F; red outlines) did not affect movement of GFP through RCs (marked with Pav::GFP). PA-GFP was activated in one cell (yellow outline) and moved through the RCs to other cells within that cyst (white outline). (G-I) PA-GFP movement occurred through RCs in elongated spermatids even after disruption of the fusome with *αSpec RNAi*.

Table

Table 1. Summary Table of Protein Movement. Fluorescence Loss in Photobleaching (FLIP) demonstrates that some GFP-tagged proteins readily move between the cells in a 16-cell cyst. GFP size is not included in the kDa calculation for each FlyTrap protein.

Protein	Size (kDa)	Function	FLIP?
GFP	27	Fluorescent protein	Yes
Kra	49	Translational regulator	Yes
Men-B	69	Metabolism enzyme	Yes
Oda	28	Antizyme	Yes
β-Tub56D	51	Cytoskeletal constituent	Yes
CaM	17	Calcium-binding messenger protein	No
Clu	161	Cytoplasmic ribonucleoprotein	No
CG32701	33	ER protein	No
eIF4A	46	Eukaryotic translation initiation factor	No
eIF4E1	46	Eukaryotic translation initiation factor	No
Lost	60	RNA metabolism protein	No
Mito-GFP		Mitochondrial targeting sequence	No
Pdcd4	56	Stem cell differentiation	No
Sgg	59	Glycogen synthase kinase 3	No
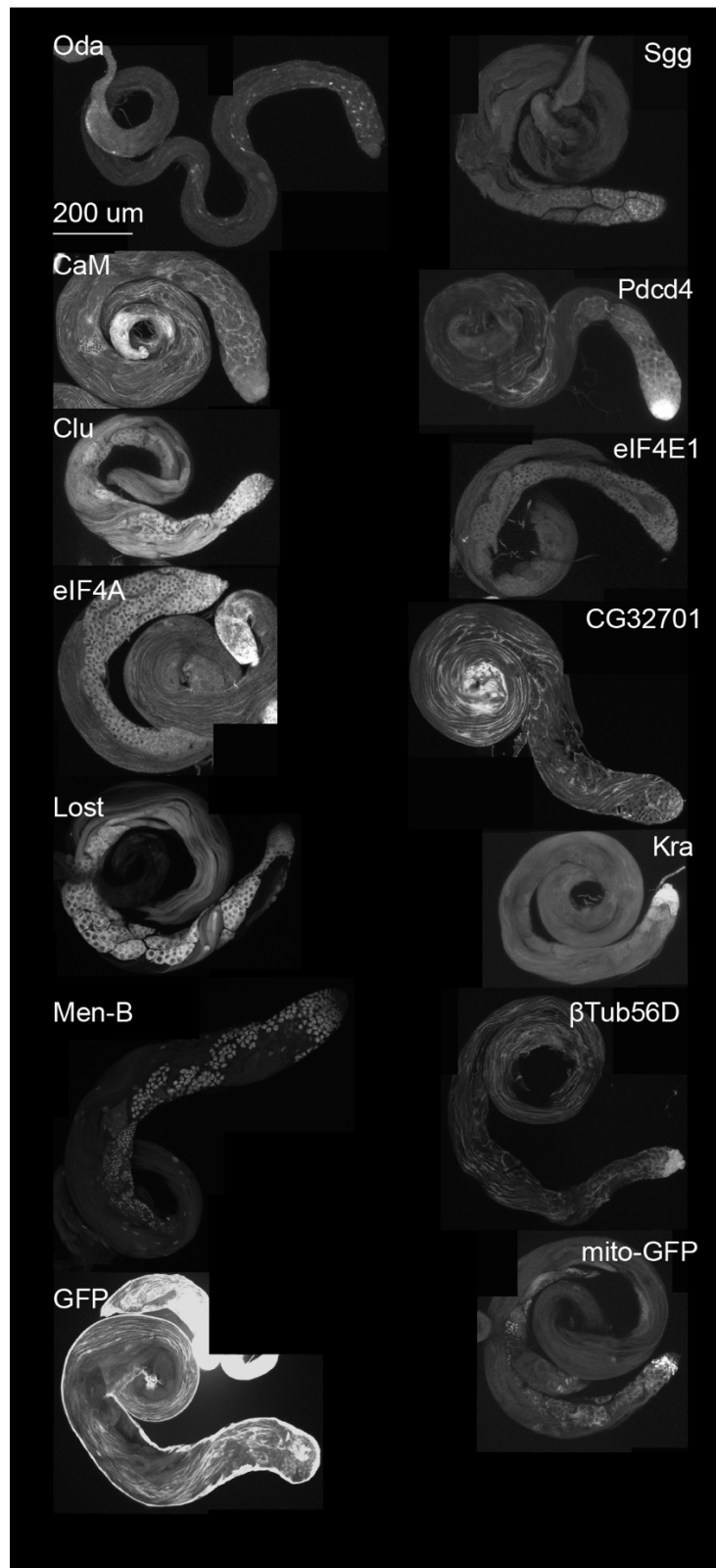
Figure S1. GFP expression pattern of FlyTrap lines used in FLIP imaging. Whole mount testes of each of the protein traps used for FLIP imaging to demonstrate differing patterns and levels of GFP expression.
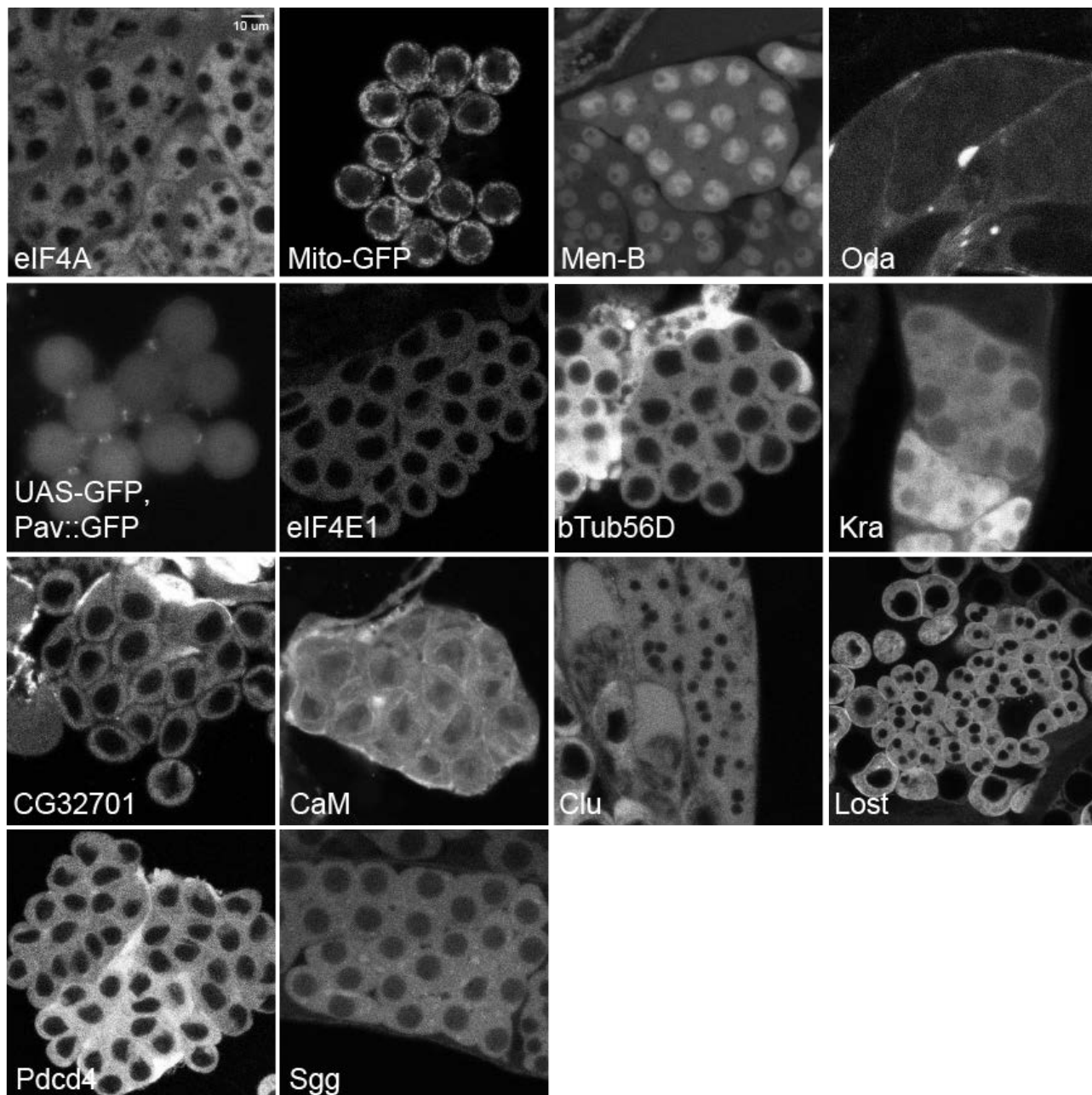
Figure S2. Expression in 16-cell cysts of all FlyTrap lines used for FLIP. Fixed examples of 16-cell cysts of each of the protein traps used for FLIP imaging to demonstrate differing patterns and levels of GFP expression.
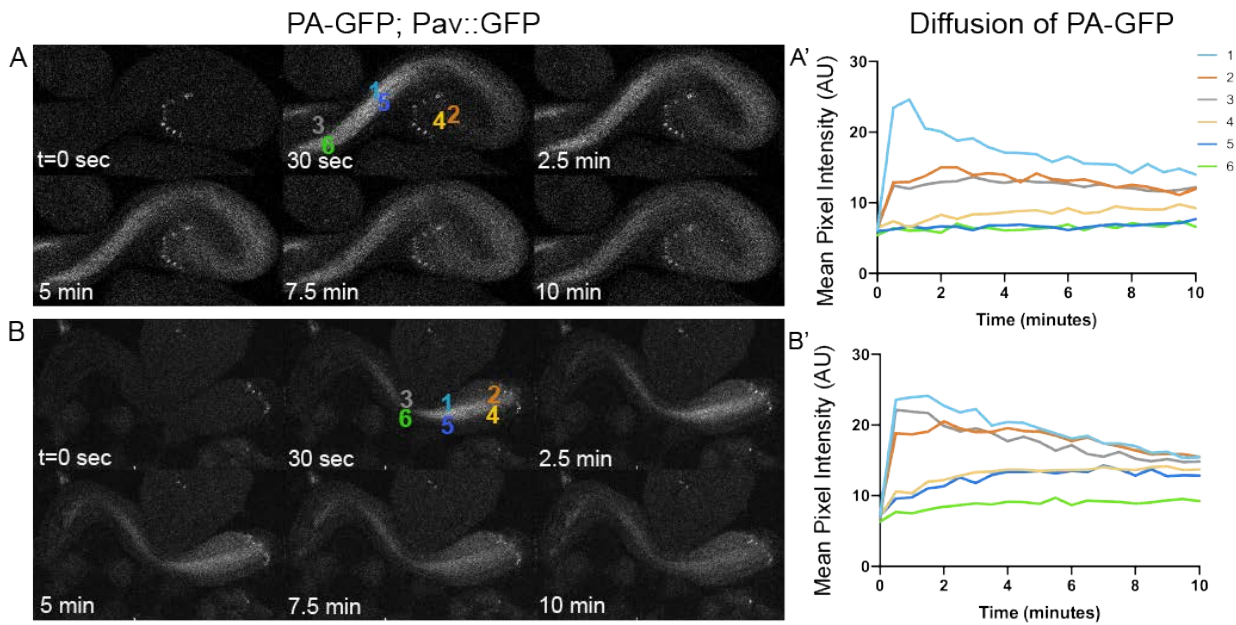
Figure S3. Movement of PA-GFP occurs through the RCs faster than through the tail perforations. (A-B) Still images of 10-minute movies capturing movement of PA-GFP in spermatid tails after activation in region 1. (A'-B') Quantification of PA-GFP fluorescence in several different locations along the spermatid tails show that PA-GFP is first observed near the RCs (region 4) rather than having traveled through the perforations (region 5).
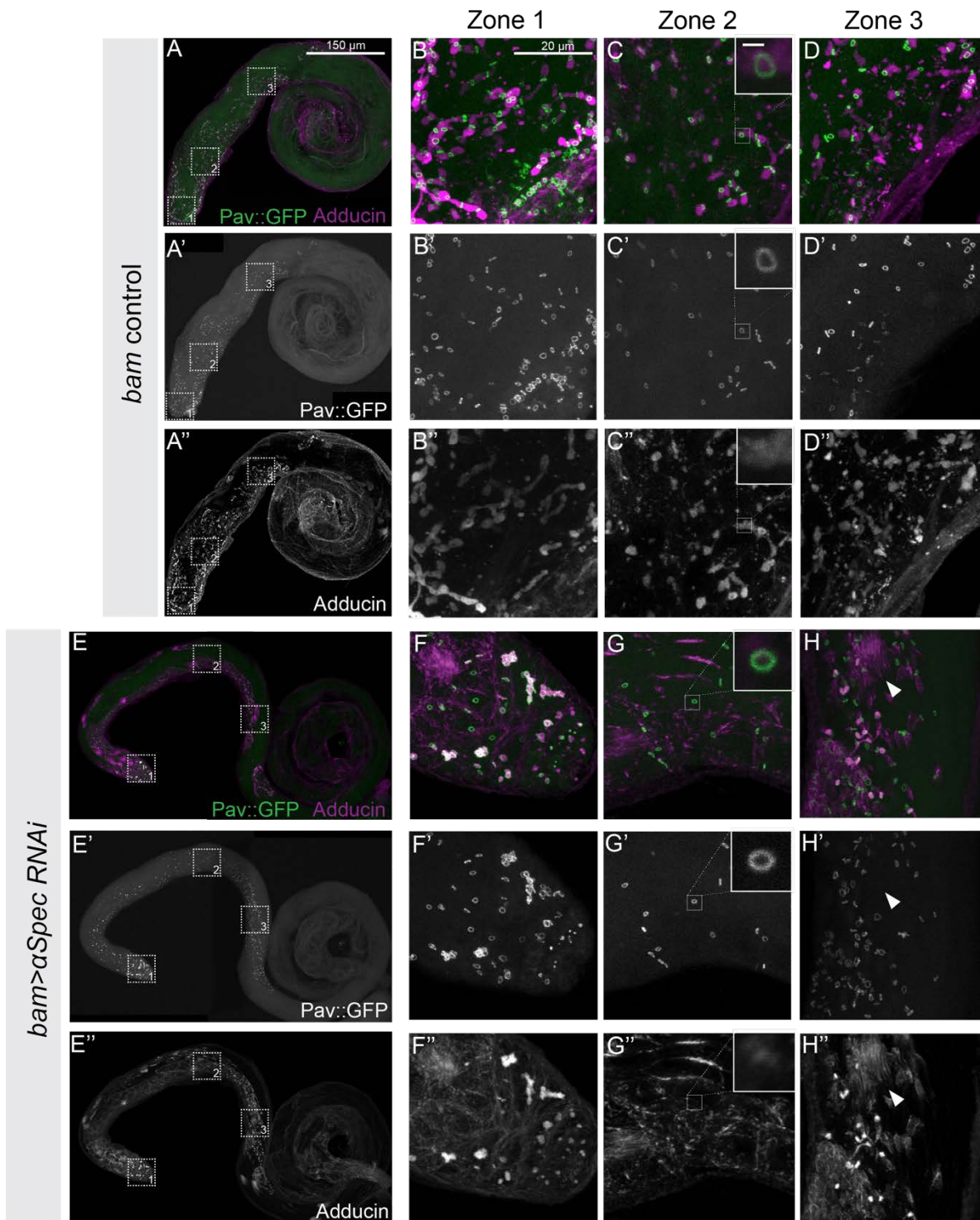
Figure S4. Fusome disruption by RNAi against α*Spectrin* using *bam-Gal4* (Adducin staining). (A) Wild-type testis with RCs marked by Pav::GFP and fusomes labeled with Adducin antibody (1B1). (B-D) Closeups of the regions marked by box in (A), highlighting the RCs (Pav, green) and fusome (Adducin, purple) in a wild-type testis in three different stages of development: mitotic (Zone 1), post-mitotic (Zone 2), and elongated spermatids (Zone 3). Insets in (C-C") highlight one RC, scale bar is 1 um. (E) Testes with α*Spectrin* RNAi lack Adducin staining at the fusome, but testis morphology appears unaffected. (F-H) Closeups of the regions marked in (E) showing Hts1B1 staining at the membrane rather than in a fusome pattern while Pav::GFP remained localized to the RCs. Small fusome-like fragments were observed in Zones 2 and 3.
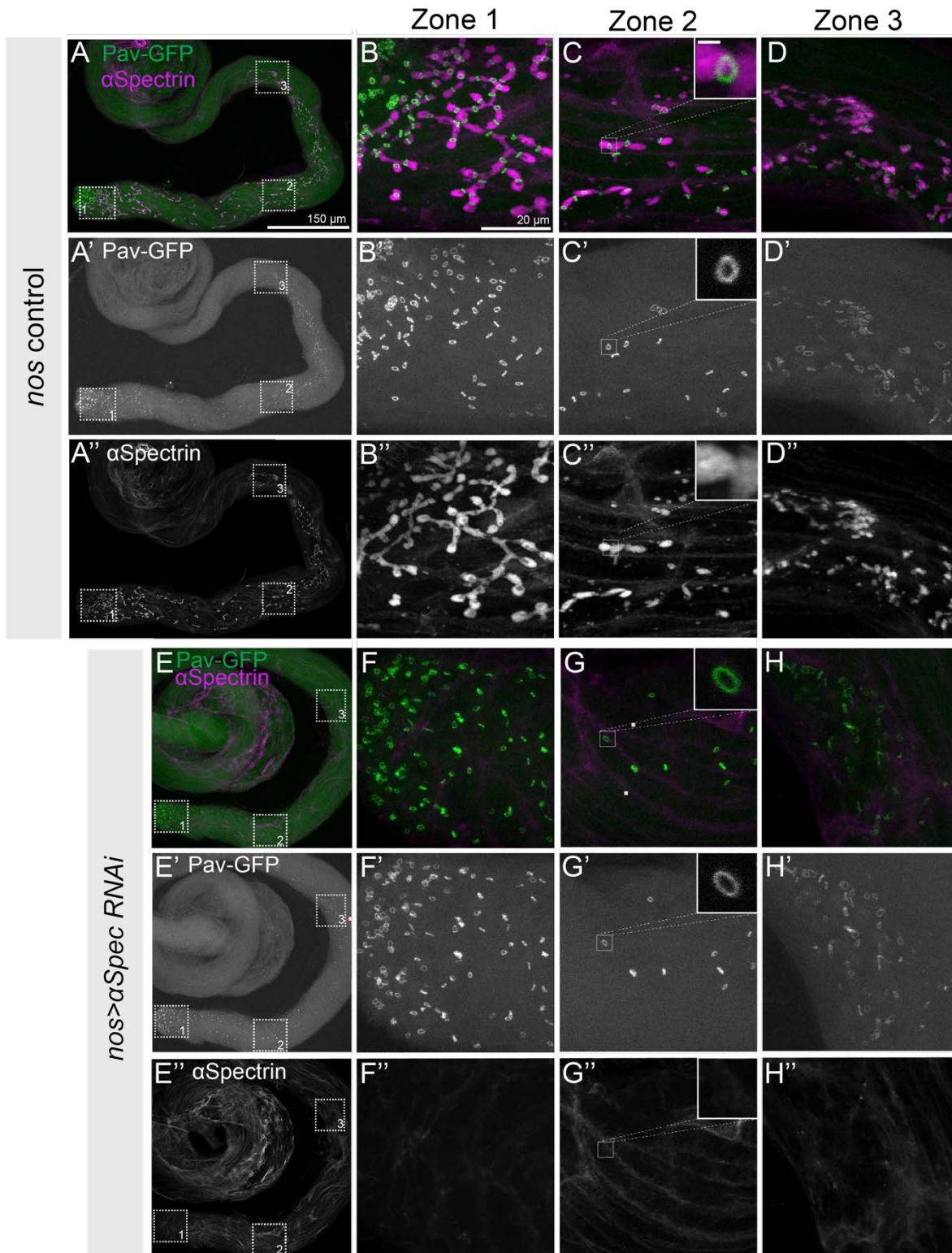
Figure S5. Fusome disruption by RNAi against α*Spectrin* using *nos-Gal4* (αSpectrin staining). (A) Wholemount Pav::GFP testis stained with αSpectrin antibody showed staining of the fusome similar to Hts1B1 (Adducin) antibody. (B-D) Close up of regions marked in (A) showing αSpectrin staining at wild-type RCs (B'-D') and the fusome (B"-D") at various stages of sperm development. (E) Disruption of fusome using *nos-Gal4>αSpectrin* RNAi showed a lack of αSpectrin staining at the fusome, but gross testis morphology appears unaffected. (F-H) Close up of insets from (E) showing intact RCs (F'-H') despite loss of αSpectrin staining (F"-H").)
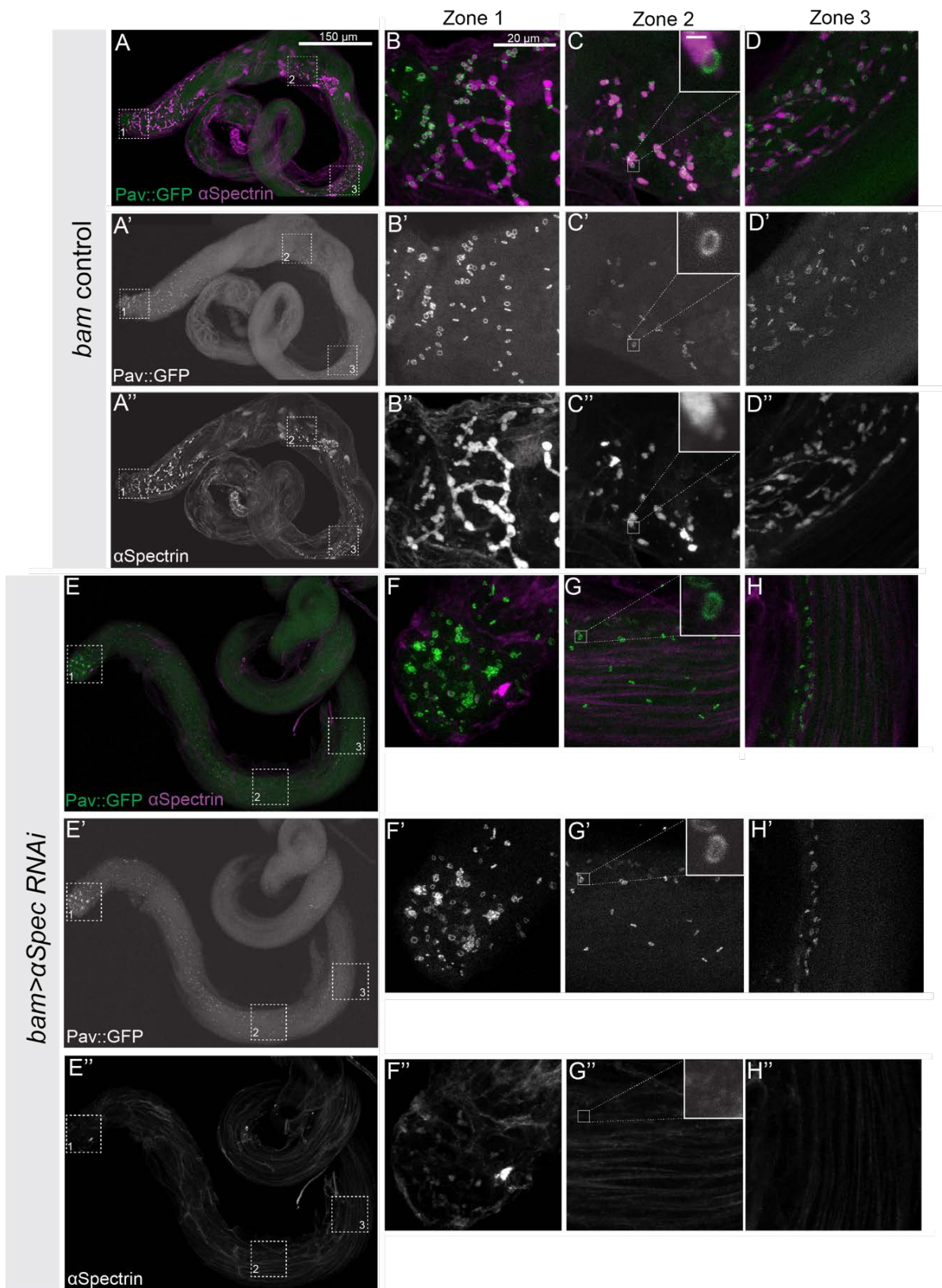
Figure S6. Fusome disruption by RNAi against αSpectrin using bam-Gal4 (αSpectrin staining). (A) αSpectrin showed staining of the fusome similar to Hts1B1 (Adducin) antibody. (B-D) Close up of regions marked in (A) showing αSpectrin staining at wild-type RCs (B'-D') and the fusome (B"-D") at various stages of sperm development. (E) Disruption of fusome using *bam-Gal4>αSpectrin* RNAi showed a lack of αSpectrin staining at the fusome, but gross testis morphology appears unaffected. (F-H) Close up of insets from (E) showing intact RCs (F'-H') despite loss of αSpectrin staining (F"-H").
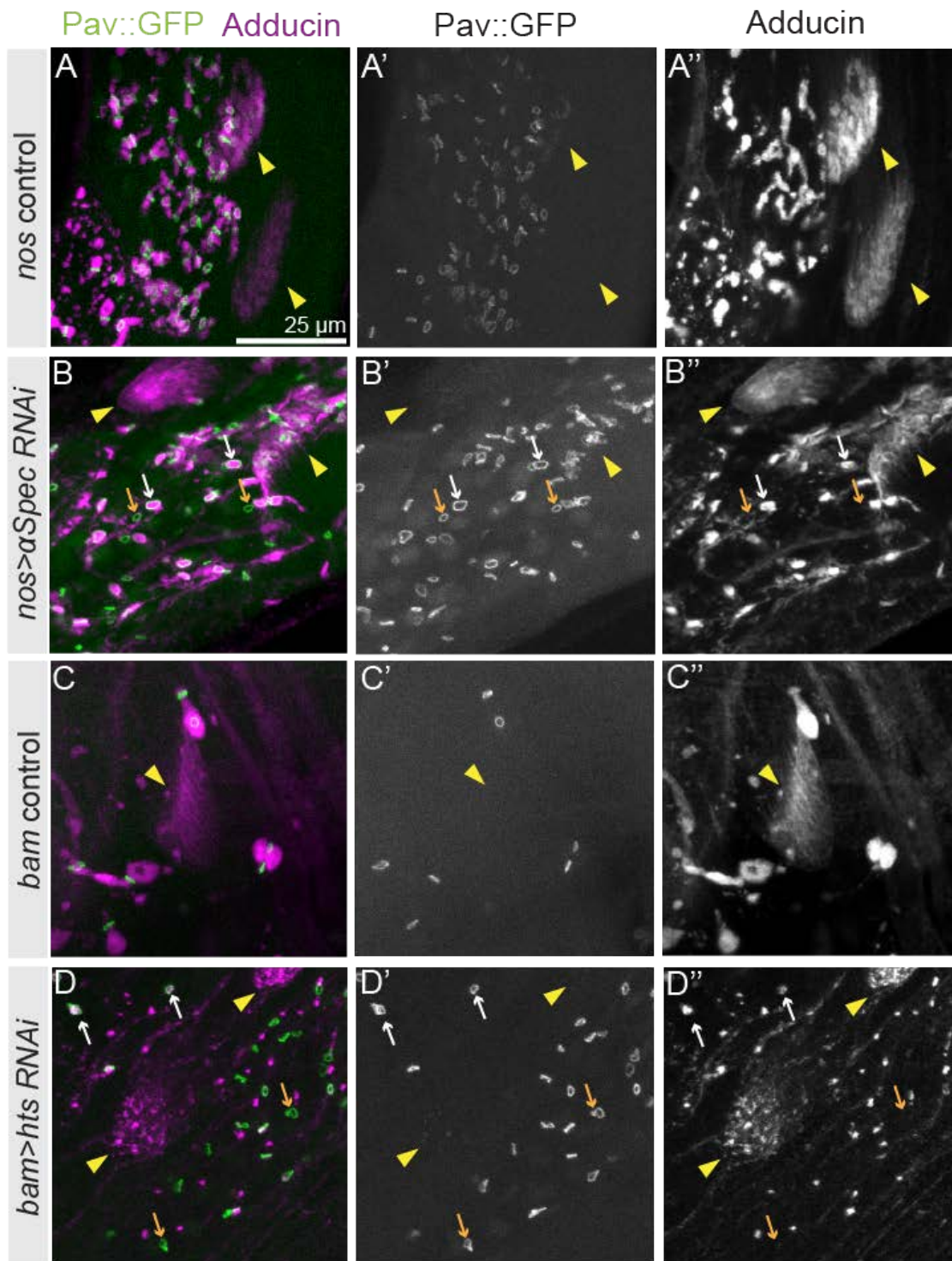
Figure S7. Knockdown of αSpec and Hts compromises the fusome but does not alter the localization of Adducin at elongating spermatid tails. Knockdown of αSpec and Hts compromises the fusome but does not alter the localization of Adducin at elongating spermatid tails. (A,C) *nos-Gal4* or *bam-Gal4* control testes (Zone 2) with RCs marked by Pav::GFP; fusomes and elongating spermatid tails (yellow arrowhead) labeled with Adducin antibody. (B) *nos>αSpec RNAi* testis showing fragmented fusomes and RCs that both associate with (white arrow) and fail to associate with (orange arrow) fusomes. (D) *bam>hts RNAi* testis showing fragmented fusomes and fragmented Adducin signal at the elongating spermatid tails. The majority of Pav::GFP-labeled RCs are not associated with the fusome fragments.
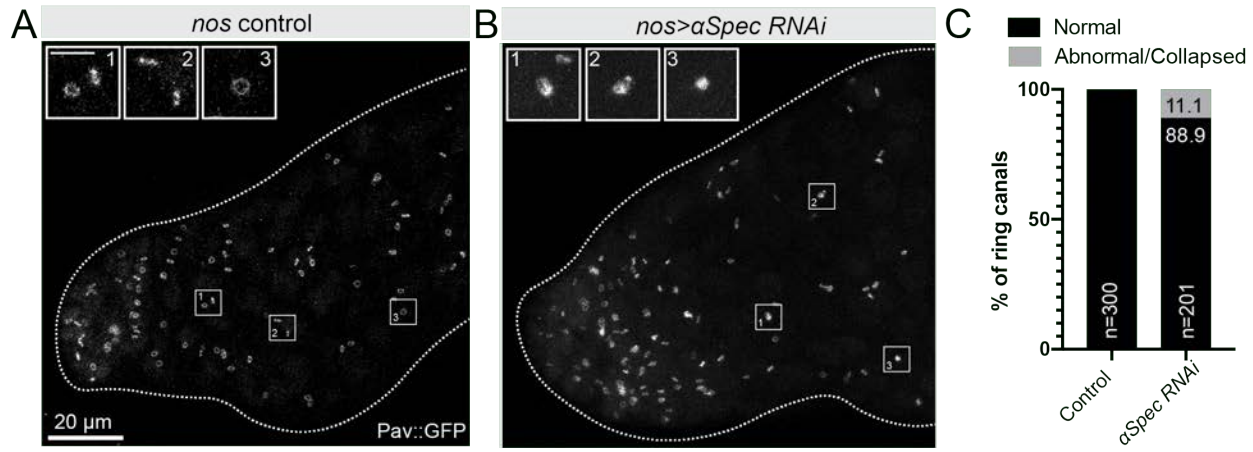
Figure S8. RC morphology following fusome knockdown (A, B). *nos-Gal4* control or *nos>aSpec RNAi* testes expressing Pav::GFP. (A) Boxed RCs are shown in the insets. Scale bar is 5 microns. (B) Abnormal or collapsed RCs highlighted in the insets. (C) Quantification of RC morphology.
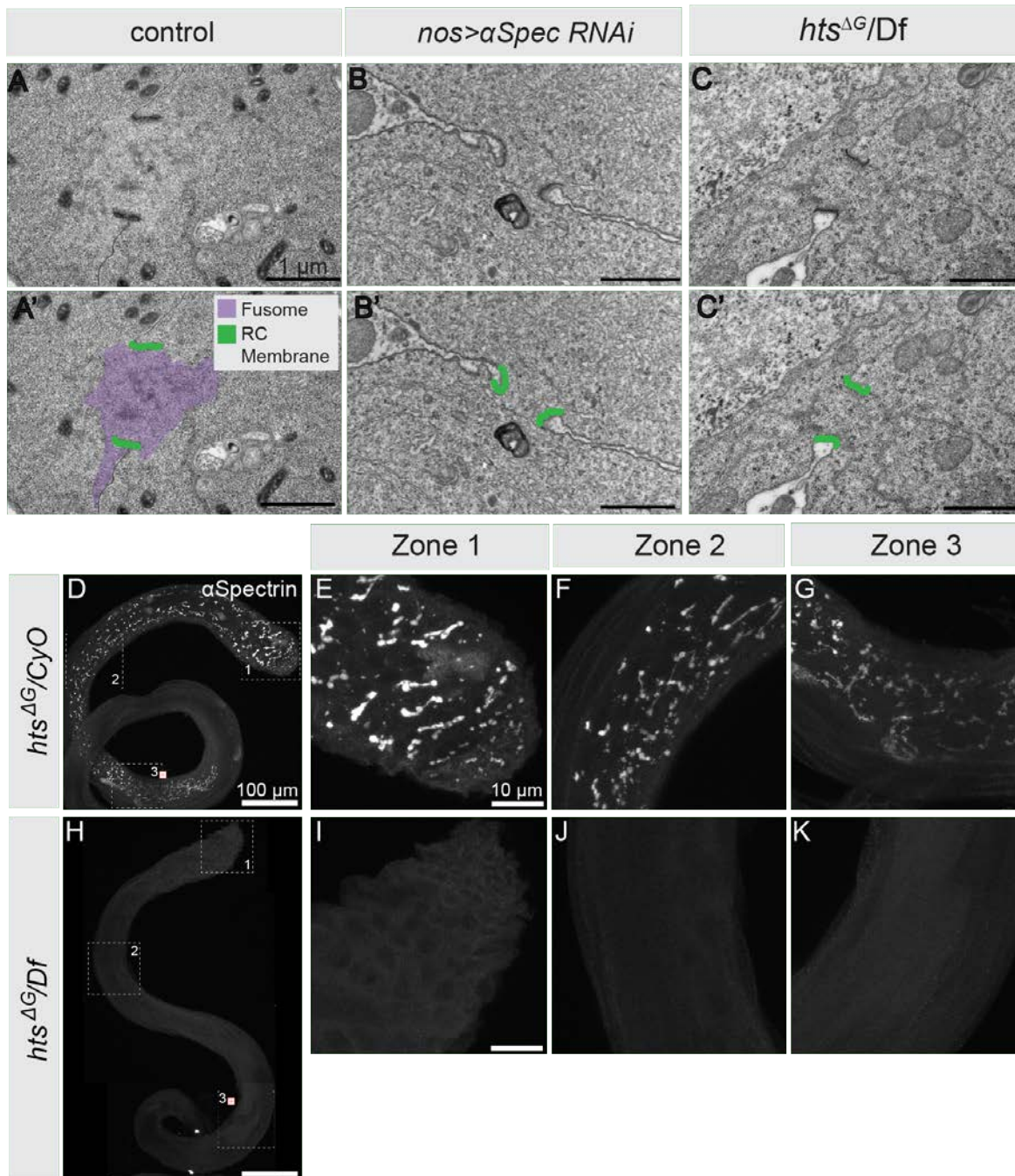
Figure S9. Additional EM showing clear fusome in wild type and compromised fusome in *αSpectrin* RNAi and *hts^{ΔG}* mutant testes. (A) EM of Pav::GFP testes showing RCs surrounding the fusome, a clear ribosome deficient cloud. (A') False coloring of (A) highlighting the fusome area (purple) and RCs (green). (B) EM pictures of *nos>αSpectrin* RNAi showing a lack of clearly marked fusome between the electron dense RCs. (C) EM images of *hts^{ΔG}/Df* testes, which show no fusome structure but intact RCs. (D) Immunofluorescence of *hts^{ΔG}/CyO* testis stained with *αSpectrin* antibody. (E-G) Insets from (D) highlighting the presence of the fusome in various stages of spermatogonial development. (H) Immunofluorescence of *hts^{ΔG}/Df* shows a lack of *αSpectrin* staining at a fusome, but spermatogenesis and testis morphology appear unaffected. (I-K) Insets of (H) showing a distinct lack of *αSpectrin* antibody staining during mitotic, post-mitotic, and spermatid elongation stages.
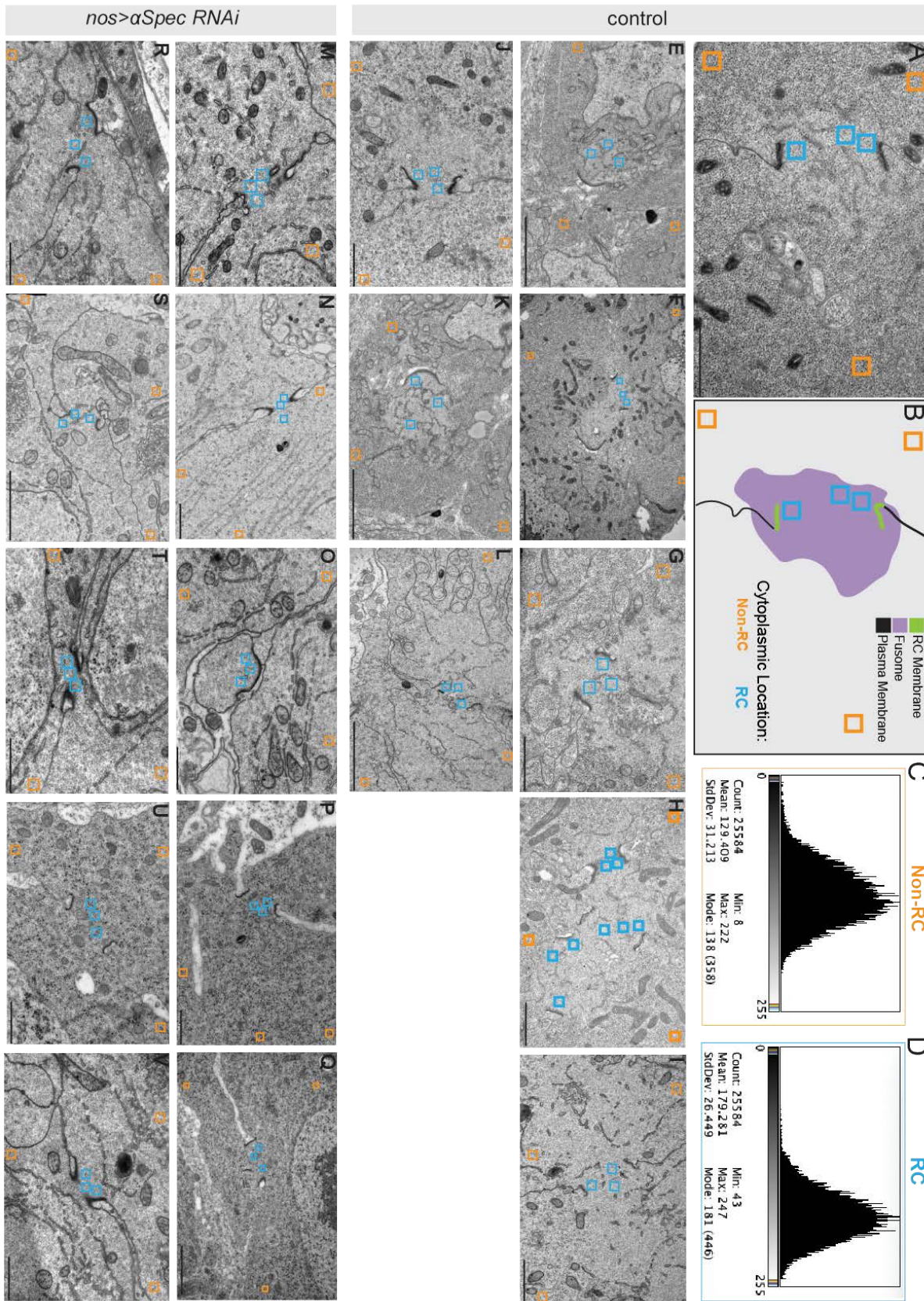
Figure S10. Additional TEM micrographs of control and *nos>aSpec RNAi* RCs. (A) Control RC with labeled ROIs (blue boxes mark RC cytoplasm; orange boxes mark non-RC cytoplasm) used for quantification of ribosome density. (B) Schematic of RC represented in (A) to mark the RC membrane (green), fusome (purple), plasma membrane (black). (C, D) Example histograms obtained from a single ROI in either the non-RC cytoplasm (orange) or RC cytoplasm (blue). (E-L) Electron micrographs of control RCs from which ribosome density measurements were obtained with labeled ROIs. (M) Electron micrographs of *nos>aSpec RNAi* RCs; measured ROIs are labeled.
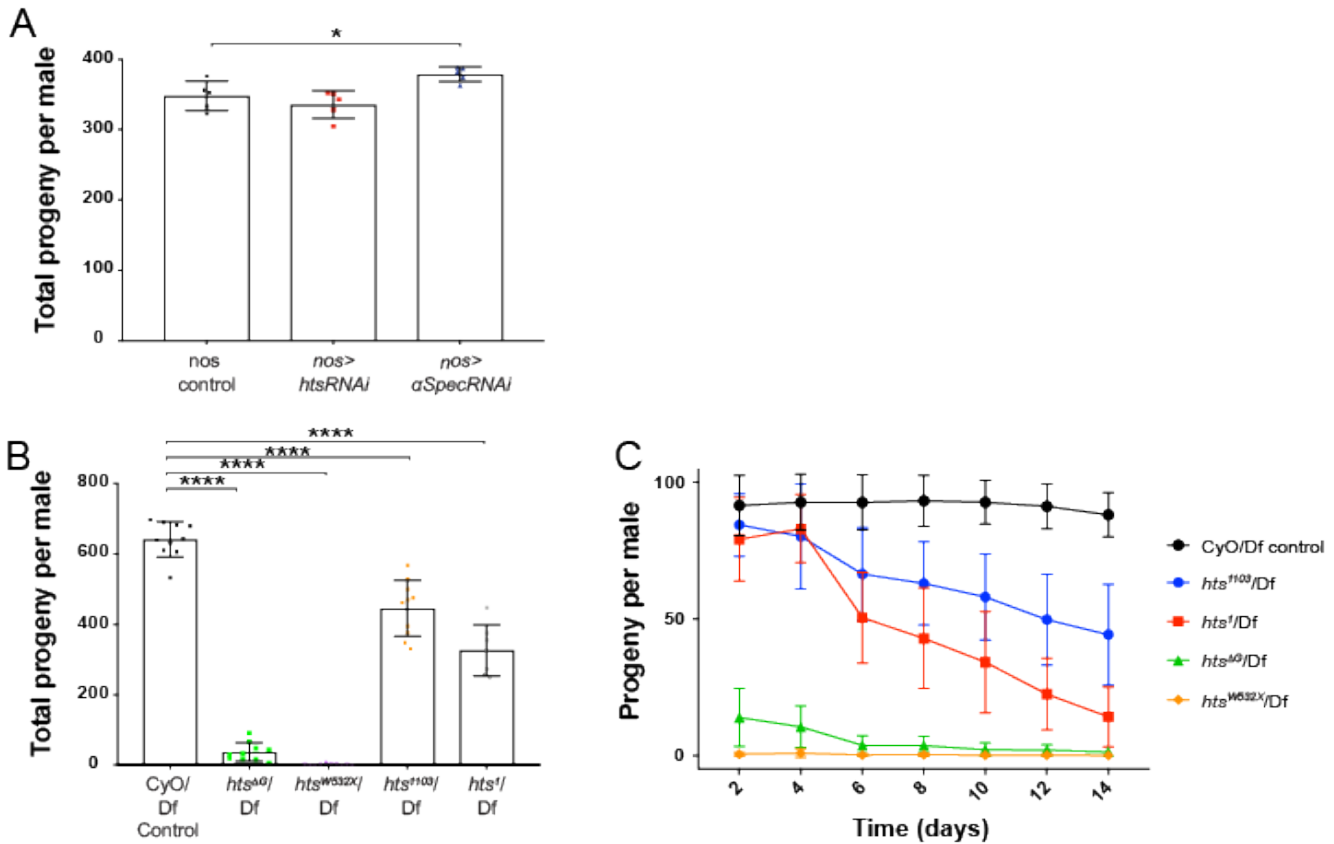
Figure S11. Fusome knockdown by germline specific RNAi does not have an effect on fertility. (A) Comparison of fertility (over a two-week period) as measured by total progeny per male between germline specific *nos-Gal4* control and *nos-Gal4* driving *hts* (p=0.45) or *aSpectrin* RNAi (p=0.03) showed a slight increase in fertility in the αSpectrin RNAi line. (B) Fertility assessment using hts alleles *htsΔG/Df*, *htsW532X/Df*, *hts1103/Df* and *hts1/Df* showed significant decrease in fertility compared to control (p<0.0001). (C) Fertility of hts1103/Df and hts1/Df decline over time in comparison to control. *htsΔG/Df* and *htsW532X/Df* were consistently less fertile than controls.
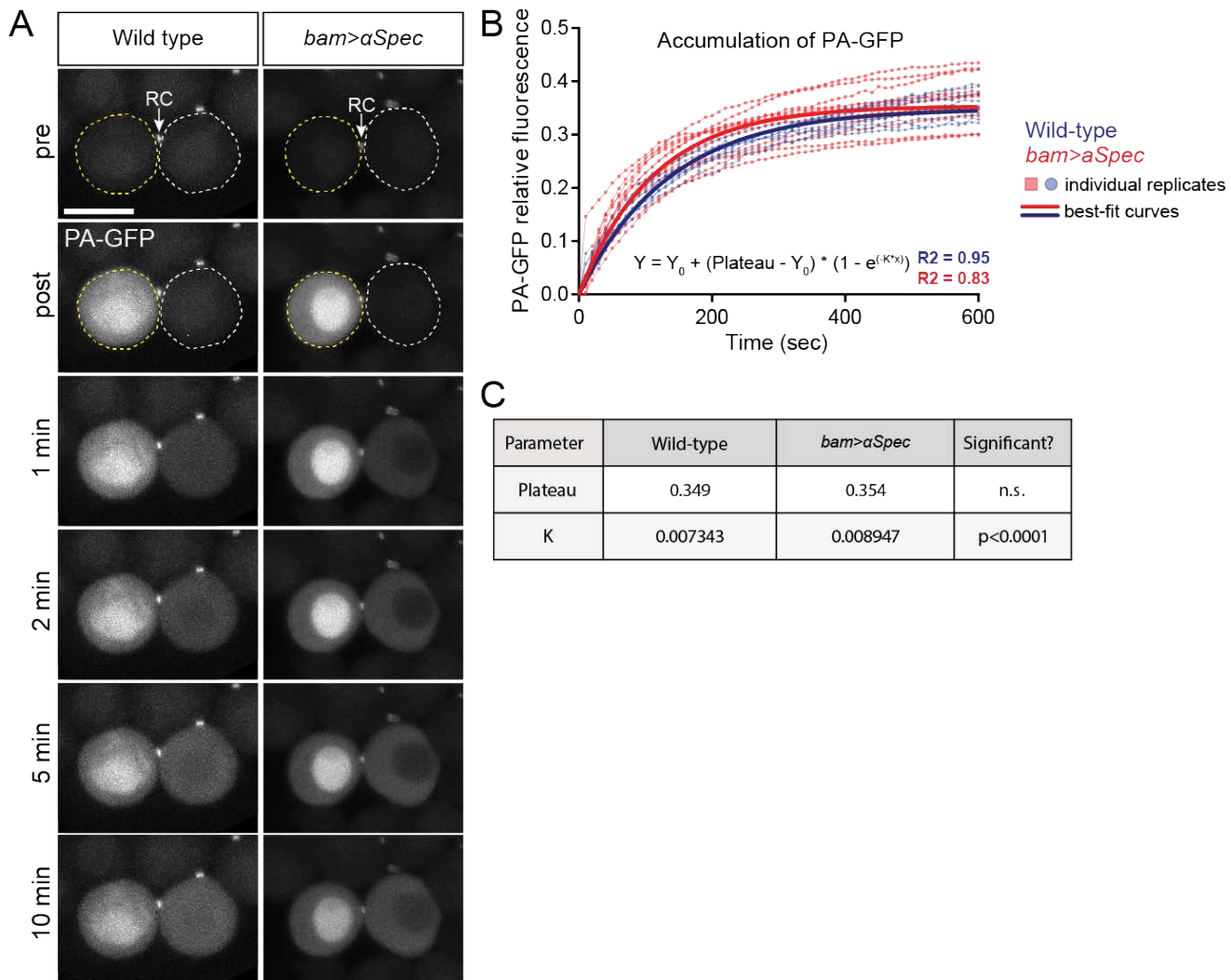
Figure S12. Movement of PA-GFP through RCs in fusome-disrupted cells is faster than in wild-type cells.
(A) A single cell expressing PA-GFP within a spermatocyte cyst was activated (yellow dashed outline) and PA-GFP fluorescence between the activated and recipient cell (white dashed outline) was imaged throughout a 10-minute time course in wild-type and fusome knockdown testes. Arrows indicate the RC, marked by Pav::GFP. Two-cell groups were selected for quantification, meaning that only movies in which PA-GFP diffused into a single adjacent cell were used for analysis. (B-C) Non-linear regression of PA-GFP RFU mean values (dashed lines) and fitted curves (solid lines) for both wild-type (blue lines) and fusome RNAi (red lines) testes. Both curves plateaued at the same RFU, but the rate of movement (as measured by the K rate constant parameter) in fusome RNAi was significantly faster than in wild-type (p<0.0001). wild-type: n=9; fusome RNAi: n=11. Scale bar = 20 μm.
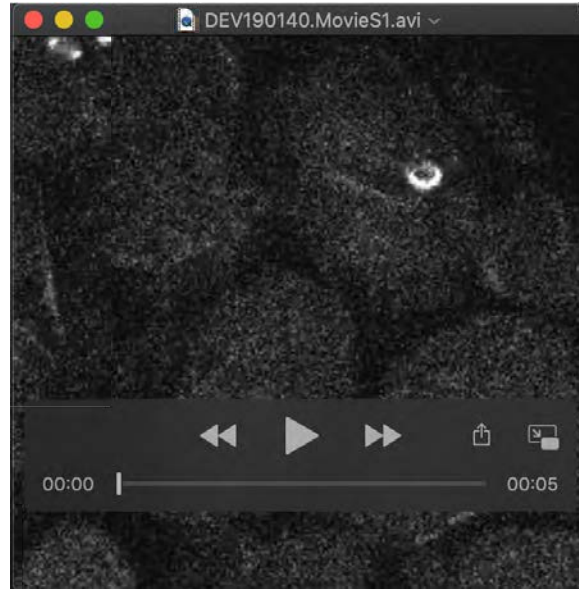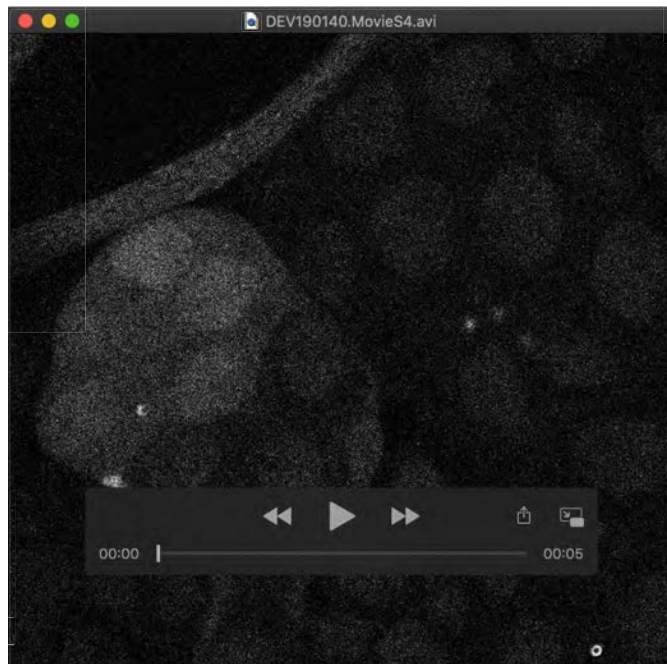
Movie 1: Movie showing movement of PA-GFP through the RCs in a 2-cell spermatogonial cyst. Photoactivation of PA-GFP in a single cell of two 2-cell spermatogonial cysts demonstrates intercellular exchange of cytoplasmic protein. Images were acquired at 30 second intervals for 10 minutes following activation.
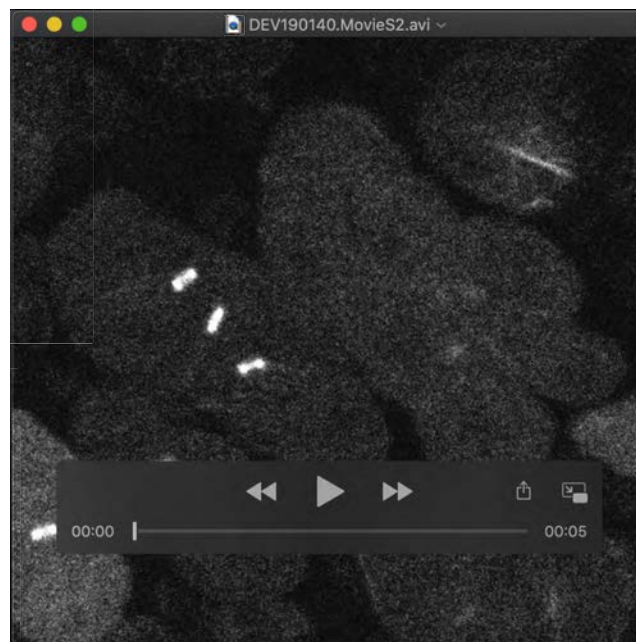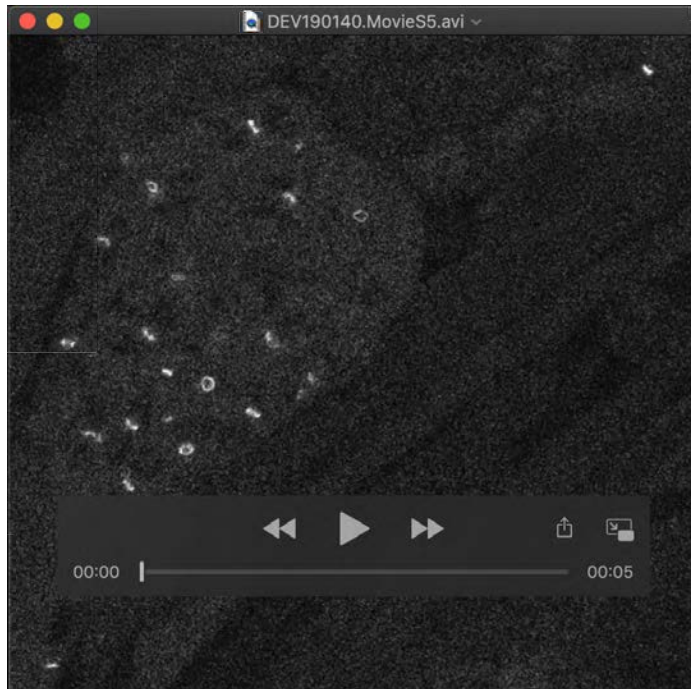

Movie 2: Movie showing movement of PA-GFP through the RCs in a 4-cell spermatogonial cyst. Photoactivation of PA-GFP in a single cell of a 4-cell spermatogonial cyst demonstrates rapid intercellular exchange of GFP. Images were acquired at 30 second intervals for 10 minutes following activation.
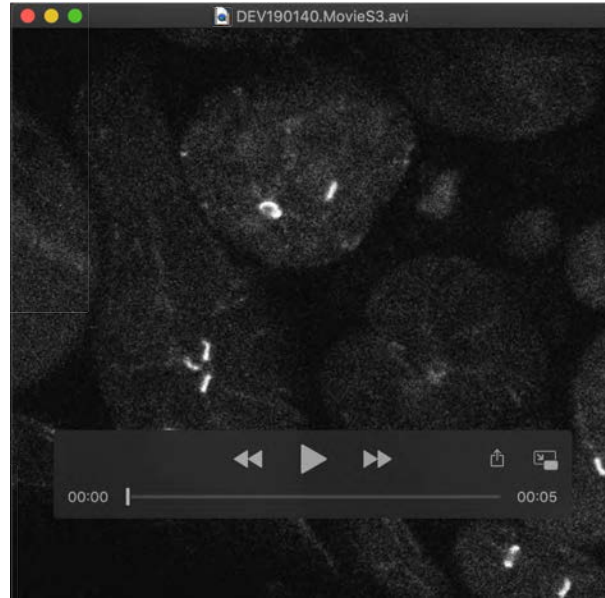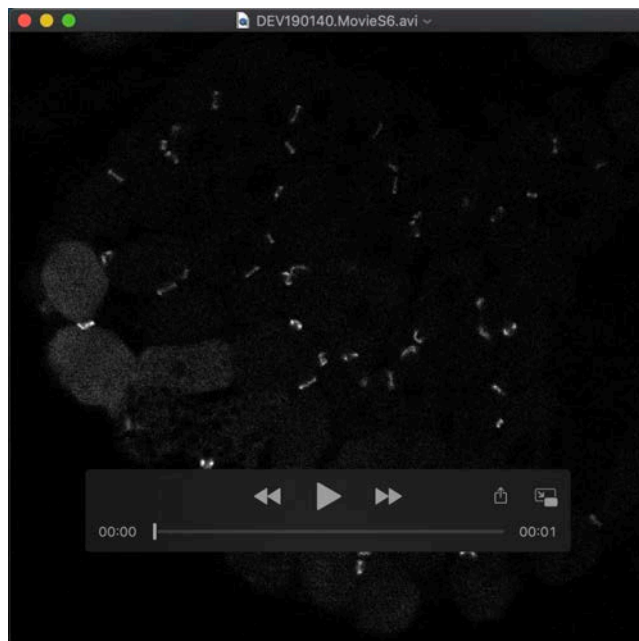
Movie 3: Movie showing movement of PA-GFP through the RCs in an 8-cell spermatogonial cyst. Photoactivation of PA-GFP in a single cell of an 8-cell spermatogonial cyst demonstrates intercellular exchange GFP through RCs in later stage mitotic cysts. Images were acquired at 30 second intervals for 10 minutes following activation.
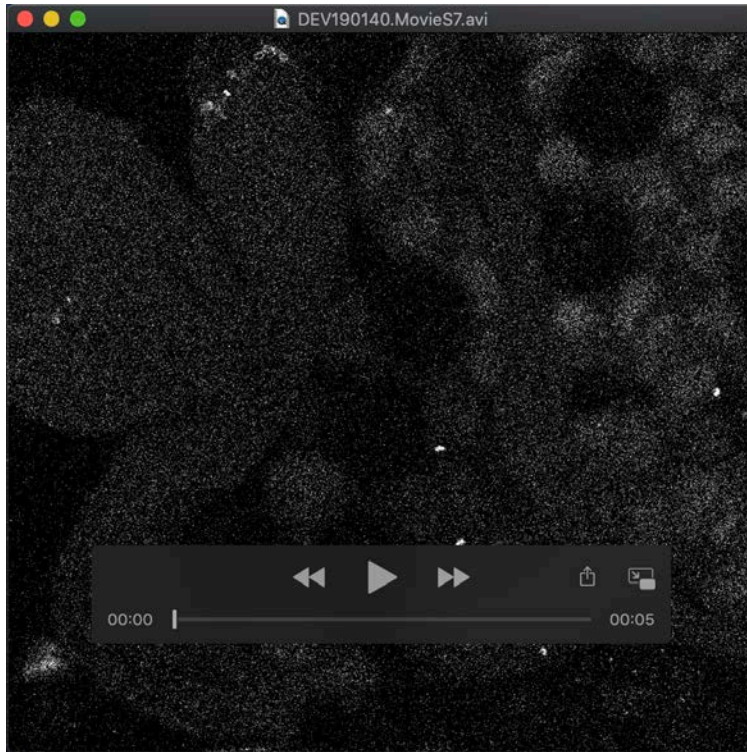

Movie 4: Movie showing movement of PA-GFP through the RCs in a 16-cell spermatocyte cyst. Photoactivation of PA-GFP in a single, center cell of a 16-cell primary spermatocyte cyst demonstrates intercellular exchange of cytoplasmic protein occurs even in cysts undergoing a growth phase. Images were acquired at 30 second intervals for 10 minutes following activation.

Movie 5: Movie showing movement of PA-GFP through the RCs in a 32-cell cyst. Photoactivation of PA-GFP in several cells of a 32-cell cyst demonstrates intercellular exchange of cytoplasmic protein happens during meiosis. Images were acquired at 30 second intervals for 10 minutes following activation.

Movie 6: Movie showing movement of PA-GFP through the RCs in a 64-cell cyst. Photoactivation of PA-GFP in 2 single cells of a 64-cell post-meiotic cyst demonstrates protein exchange occurs post-meiotically. Images were acquired at 30 second intervals for 10 minutes following activation.
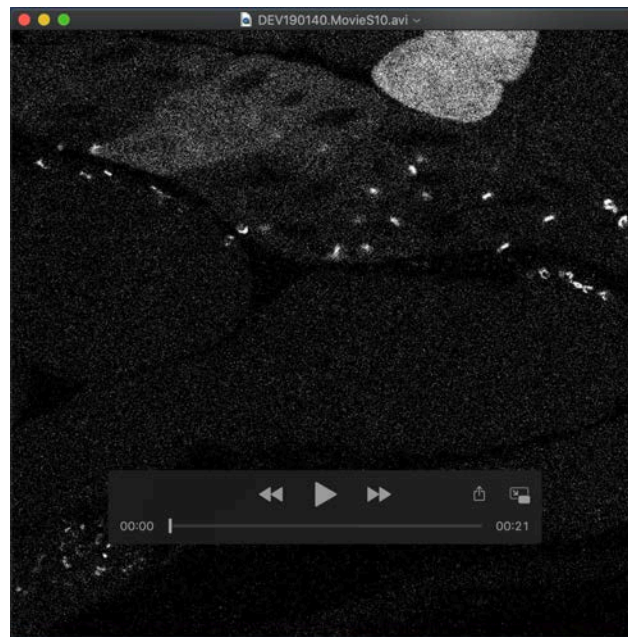
Movie 7: Movie showing movement of PA-GFP through the RCs in elongating spermatids. Photoactivation of PA-GFP in a subset of spermatids demonstrates intercellular exchange of cytoplasmic protein occurs post-tail elongation. Images were acquired at 30 second intervals for 10 minutes following activation.

Movie 8: Moving showing movement of PA-GFP through the RCs in 2- and 4-cell spermatogonial cysts lacking a fusome. Photoactivation of PA-GFP in single cells of 2- and 4-cell spermatogonial cysts in *nos-Gal4>aSpectrin* RNAi testes demonstrates intercellular exchange of cytoplasmic protein occurs despite the lack of fusome structure. Images were acquired at 30 second intervals for 10 minutes following activation.

Movie 9: Movie showing movement of PA-GFP through the RCs in a 16-cell spermatocyte cyst lacking a fusome. Photoactivation of PA-GFP in a single cell of 16-cell spermatocyte cyst in *bam-Gal4>αSpectrin* RNAi testes demonstrates intercellular exchange of PA-GFP is not mediated by the fusome in primary spermatocytes. Images were acquired at 30 second intervals for 10 minutes following activation.

Movie 10: Movie showing movement of PA-GFP through the RCs in a spermatids lacking a fusome. Photoactivation of PA-GFP in a subset of spermatids in *bam-Gal4>αSpectrin* RNAi testes demonstrates intercellular exchange of PA-GFP is not mediated by the fusome post-meiotically. Images were acquired at 30 second intervals for 40 minutes following activation.

Reagents Table

REAGENT or RESOURCE	SOURCE	IDENTIFIER
Antibodies		
Mouse monoclonal anti-Hts (1B1)	Developmental Studies Hybridoma Bank	Cat#1b1, RRID:AB_528070
Mouse monoclonal anti-αSpec (3A9)	Developmental Studies Hybridoma Bank	Cat#3A9 (323 or M10-2), RRID:AB_528473
Goat anti-mouse IgG Secondary Antibody, Alexa Fluor 568	Thermo Fisher Scientific	Cat#A-11031, RRID: AB_144696
Chemicals and Recombinant Protein		
Paraformaldehyde, 16% solution, EM grade	VWR	Cat#15710-S
Bovine Serum Albumin	AmericanBio	Cat#AB01088
Triton X-100	AmericanBio	Cat#AB02025-00500
ProLong Gold Antifade Mountant	Thermo Fisher Scientific	Cat#P36934
Aqua-Poly/Mount	Polysciences, Inc.	Cat#18606
Experimental Models		
D. melanogaster: pJFRC92-20XUAS-IVS-Syn21-mC3PAGFP-p10	Laboratory of G. Rubin; Pfeiffer et al. 2012	N/A
D. melanogaster: Bam-Gal4: W1118; P[Bam-Gal4:VP16]	Labortory of D. McKearin; Chen & McKearin 2003	N/A
D. melanogaster: htsΔG	Zuker collection, Koundakjian et al., 2004	FlyBase ID: FBal0212993
D. melanogaster: Tub-Gal4: y1 w*; P{w+mC=tubP-GAL4}LL7/TM3, Sb1 Ser1	Bloomington Drosophila Stock Center	RRID:BDSC_5138
D. melanogaster: Nos-Gal4: P{w+mC=GAL4::VP16-nos.UTR}MVD2, w1118	Bloomington Drosophila Stock Center	RRID:BDSC_7303
D. melanogaster: αSpectrin shRNA: y1 sc* v1; P{y+t7.7 v+t1.8=TRiP.HMC04371}attP40	Bloomington Drosophila Stock Center	RRID:BDSC_56932
D. melanogaster: hts Df: w[1118]; Df(2R)BSC135/CyO	Bloomington Drosophila Stock Center	RRID: BDSC_9423
D. melanogaster: JFRC81- 10XUAS-IVS-Syn21-GFP-p10	Laboratory of G. Rubin; Pfeiffer et al. 2012	N/A
D. melanogaster: Cam::GFP	Laboratory of L. Cooley; Kelso et al. 2004	YC0069LE
D. melanogaster: Clu::GFP: w1118; P{w+mC=PTT-GA}cluG00271	Bloomington Drosophila Stock Center	RRID:BDSC_6842
D. melanogaster: EIF4α::GFP	Laboratory of L. Cooley; Kelso et al. 2004	YC0001
D. melanogaster: EIF4E1::GFP: y1 w*/Dp(1;Y)y+; P{w+mC=PTT-GC}eIF4E1YC0001	Bloomington Drosophila Stock Center	RRID:BDSC_50858
D. melanogaster: G0320::GFP: w* P{w+mC=PTT-un1}l(1)G0320^{G00024}	Bloomington Drosophila Stock Center	RRID:BDSC_50839
D. melanogaster: Lost::GFP: w1118; P{w+mC=PTT-GA}lostZCL3169	Bloomington Drosophila Stock Center	RRID:BDSC_6832
D. melanogaster: Mito::GFP: w1118; P{w+mC=UAS-mito-HA-GFP.AP}2/CyO	Bloomington Drosophila Stock Center	RRID:BDSC_8442
D. melanogaster: Pdcd4::GFP: w1118 P{w+mC=PTT-GB}Pdcd4G93	Bloomington Drosophila Stock Center	RRID:BDSC_38446
D. melanogaster: Sgg::GFP: y1 P{w+mC=PTT-un1}sggZCL1912 w*	Bloomington Drosophila Stock Center	RRID:BDSC_50887
D. melanogaster: Kra::GFP: y1 w*; l(2)**/In(2LR)Gla, wgGla-1; PBac{y+mDint2=HpaI-GFP.A}kraYD0086/TM6C, Sb1	Bloomington Drosophila Stock Center	RRID:BDSC_50873
D. melanogaster: Men-B::GFP: w*; l(2)**/In(2LR)Gla, wgGla-1; P{w+mC=PTT-GB}Men-bYB0142	Bloomington Drosophila Stock Center	RRID:BDSC_50854
D. melanogaster: Oda::GFP	Laboratory of L. Cooley; Kelso et al. 2004	YD0523
D. melanogaster: βTub56D::GFP: w*; P{w+mC=PTT-GC}betaTub56DYC0063/CyO	Bloomington Drosophila Stock Center	RRID:BDSC_50867
Oligonucleotides		
Primer for HA::KnSm::FLAG (forward): TACCCCTACGACGTGCCCGACTACGCCatctggacaagggaaaacg	This study	N/A
Primer for HA::KnSm::FLAG (reverse): CTTATCGTCATCATCCTTGTAATCatctcgtgatggcaggttg	This study	N/A
Primer for HA::GFP::FLAG (forward): TACCCCTACGACGTGCCCGACTACGCCATGTCCAAAGGTGAAGAACTG	This study	N/A
Primer for HA::GFP::FLAG (reverse): TTACTTATCGTCATCATCCTTGTAATCCTTGTAGAGCTCATCCATGC	This study	N/A
Primer for insertion of KnSm cassette and HA::GFP::FLAG at the Pav c-terminus for Pav::GFP BAC transgene (forward): CCCGCTGCAATCTCGGCATTGAGGGACACAGCAGCAAGAAGTCGAAAATCTACCCCTACGACGTGCCC	This study	N/A
Primer for insertion of KnSm cassette and HA::GFP::FLAG at the Pav c-terminus for Pav::GFP BAC transgene (reverse): CTATGAACTAAATGGGTAATTGACTTTGAGAATTCCACGCTGAGTCATTTTTACTTATCGTCATCATCCTTG	This study	N/A
Recombinant DNA		
BAC CH322-102N03	CHORI	N/A
Software		
ImageJ/FIJI	NIH	https://fiji.sc/
Prism 7	GraphPad	https://www.graphpad.com/scientificsoftware/prism/
Imaris 9.0	Bitplane	http://www.bitplane.com/
Other		
Drosophila transgenesis: site-specific integration	Rainbow Transgenic Flies, Inc.	http://www.rainbowgene.com/